Available online at www.sciencedirect.com
ScienceDirect
Lithos 98 (2007) 1–26
LITHOS
www.elsevier.com/locate/lithos

High-Mg andesites and related lavas from southwest Puerto Rico (Greater Antilles Island Arc): Petrogenetic links with emplacement of the Late Cretaceous Caribbean mantle plume

Wayne T. Jolly [a,*], Johannes H. Schellekens [b], Alan P. Dickin [c]

[a] *Department of Earth Sciences, Brock University, St. Catharines, ON Canada L2S 3A1*
[b] *Department of Geology, University of Puerto Rico at Mayagüez, Mayagüez, 00681–5000 Puerto Rico*
[c] *Department of Geography and Geology, McMaster University, Hamilton, ON Canada L8S 4M1*

Received 13 June 2006; accepted 26 January 2007
Available online 8 February 2007

Abstract

Two-pyroxene-bearing high-Mg andesite, hornblende basalt and andesite, and high-Fe augite basalt were erupted simultaneously in southwest Puerto Rico between 85 and 65 Ma. An analogy with geologic settings in Cenozoic arcs indicates that hornblende-bearing lavas and high-Mg andesites, restricted to the southwestern-most corner of Puerto Rico, represent the forearc assemblage, whereas high-Fe basalts, concentrated in an adjacent volcanic belt toward the northeast, represent the arc-axis suite. This arrangement implies northeast-dipping subduction of refractory Jurassic chert from the Caribbean Basin, and is, therefore, consistent with relatively low Sr-isotope ratios in all three lava suites compared with correlative strata in Eastern Puerto Rico. Moreover, Pb- and Nd-isotope ratios and trace element melting models for both high-Mg andesites and hornblende-bearing lavas are consistent with the presence of a slab melt component generated by high-pressure fusion of incompatible element-enriched plateau basalts. The most likely source for such a basaltic component is the Caribbean basalt plateau, which is represented in southwest Puerto Rico by the Upper Cajul Formation. The models indicate that up to 5% slab melt was added to the source of hornblende-bearing lavas, but higher proportions, as much as 10%, are required to generate high-Mg andesites. The elevated buoyancy of the more enriched and siliceous high-Mg andesite source apparently destabilized the mantle wedge and induced combined mantle-mass assimilation and fractional crystallization of orthopyroxene (AFC ≈ 1), which ultimately produced elevated MgO and low Al_2O_3 concentrations characteristic of the high-Mg andesites. The tectonic setting in southwest Puerto Rico was unlike Cenozoic analogues, because the pre-arc basement was already old (Early Jurassic, 185–155 Ma) at the time of initial island arc volcanism (~85 Ma). However, geothermal gradients in the region were increased again immediately preceding arc volcanism by emplacement of the Caribbean mantle plume (92–88 Ma), during which the original N-MORB-type upper mantle in the region was replaced by incompatible element-enriched material. The elevated heat flow produced by plume emplacement, supplemented by ascent of plume basalts from depth and associated gabbroic underplating, is inferred to have promoted slab melting. The presence of a low Zr/Sm component in both plateau basalts and arc lavas in southwest Puerto Rico is consistent with the incorporation of a small biogenic supra-subduction zone component of Atlantic origin, introduced into the back-arc region of an older (from 115 Ma) southwest-dipping subduction zone in eastern Puerto Rico.

Keywords: High-Mg andesite; Slab melt; Trace element and isotope geochemistry; Caribbean mantle plume; Supra-subduction zone

* Corresponding author.
E-mail addresses: wayne@brocku.ca (W.T. Jolly), schellek@uprm.edu (J.H. Schellekens), dickin@mcmaster.ca (A.P. Dickin).

doi:10.1016/j.lithos.2007.01.011

1. Introduction

The deeply dissected Greater Antilles arc platform preserves a continuous stratigraphic record extending from Albian in the Early Cretaceous to mid-Eocene time (approximately 115 to 45 Ma; Schellekens, 1998; Jolly et al., 1998; Iturralde-Vinent and McPhee, 1999; Viruete et al., 2006), a total of at least 70 millon years. Because the volcanic geochemistry and lithological sequences are similar in all the islands, the Antilles platform is considered to be the remnants of a once continuous volcanic chain that formed in the eastern Pacific and was subsequently inserted eastward into the modern Caribbean region (Pindell et al., 2006). One of the most important unresolved tectonic problems in the Greater Antilles, as in many extinct and degraded island arc systems, is the polarity of subduction that produced the arc. As a result of the uncertainties, two contrasting models of Caribbean evolution have arisen. In one of these, the arc is associated with a northeast-dipping Cordilleran-type subduction zone that was operative until the Campanian (~80 Ma), when the original subduction zone was choked-off by approach of the Caribbean basalt plateau from the Pacific region and replaced by a new southwest-dipping subduction zone on the opposite (northeastern) flank of the arc platform (Mattson, 1979; Burke, 1988; Schellekens, 1993; Lapierre et al., 1997; Schellekens, 1998; Smith et al., 1998; Lapierre et al., 1999; Kerr et al., 1999; Révillon et al., 2000; Kerr et al., 2002; Kerr and Tarney, 2005). In the other model, the shift from northeast- to southwest-dipping subduction in the Antilles occurred earlier, during Albian time (between ~115 and 100 Ma), after which the arc platform drifted from the Pacific region eastward into the slot between the Americas overriding the embryonic Atlantic basin (Pindell and Barrett, 1990; Erikson et al., 1990; Iturralde-Vinent and McPhee, 1999; Draper et al., 1996; Lewis et al., 1999, 2002; Kesler and Campbell, 2005; Jolly et al., 2001, 2006; Pindell et al., 2006).

In the absence of unambiguous geological or geophysical evidence of ancient subduction parameters along the northeastern segment of the Antilles arc platform, an indirect approach is required to resolve the question of subduction polarity. One avenue with considerable promise is provided by the occurrence of high-Mg andesites and related lavas in southwest Puerto Rico. These rocks are significant because Cenozoic analogues are normally restricted to the forearc region of island arcs. Moreover, since high-Mg andesites are reported only from Cenozoic arcs that have anomalous elevated heat flow, their occurrence potentially provides insight not only into the polarity but also the thermal regime of ancient arc systems. One of the principal objectives of this investigation is to compare the geochemistry and tectonic setting of high-Mg andesites from southwestern Puerto Rico with analogues in Cenozoic arcs with the goal of providing constraints on the polarity of Late Cretaceous subduction in the northeast Antilles.

2. Geological setting

The long-lived Antilles Island Arc consists of two segments:1) the extinct Late Mesozoic to Paleogene Greater Antilles in the north, including Cuba, Jamaica, Hispaniola, Puerto Rico, and the Virgin Islands, and 2) the volcanically active Lesser Antilles, which rest on buried remnants of the older Mesozoic arc (Fig. 1A). Located at the northeastern end of the ancient Greater Antilles island arc platform, the Puerto Rico–Virgin Islands microplate (PRVI, Jansma et al., 2000; Bawiec, 2001), which bridges the transition between these two major segments, occupies the broad zone between the diffuse Puerto Rico Trench Thrust on the north and the Los Muertos Trench Thrust on the south, and extends almost 450 km eastward from Mona Passage to the Anegada Fault Zone (Fig. 1A).

2.1. Pre-arc basement

The entire sequence of pre-arc basement rocks is exposed in the Sierra Bermeja Complex (Mattson, 1960; Fig. 1B) of southwest Puerto Rico. The oldest rocks consist of a melange of serpentinized spinel peridotite (Frost and Schellekens, 1991; Schellekens, 1991; Schellekens et al., 1998; Jolly et al., 2001) representing depleted lithospheric mantle. The serpentinite contains abundant xenolithic clasts, up to a kilometer in diameter, of Jurassic tholeiitic pillow lava of N-MORB-type (Lower Cajul Formation, LCAJ in Figs. 1B, 2), equivalent amphibolite, and pelagic chert, which together represent tectonized pre-arc oceanic crust. Overlying the melange is at least 300 m of Mariquita Chert of early Jurassic (Pleinsbachian, 185 Ma) to mid-Cretaceous age, representing pelagic sediment of Pacific (Farallon) provenance (Montgomery et al., 1994). The uppermost unit in the basement is a sequence of massive aphanitic basalt lava flows of unknown thickness (Upper Cajul Formation, Fig. 1A), representing a local facies of the Late Cretaceous Caribbean basalt plateau (in the sense of Hauff et al., 2000; Kerr et al., 2002). Two additional northeast-trending ultramafic belts, the Río Guanajibo serpentinite belt and Monte del Estado serpentinized peridotite, effectively subdivide southwestern Puerto Rico into three isolated tectonic blocks (Fig. 1B).

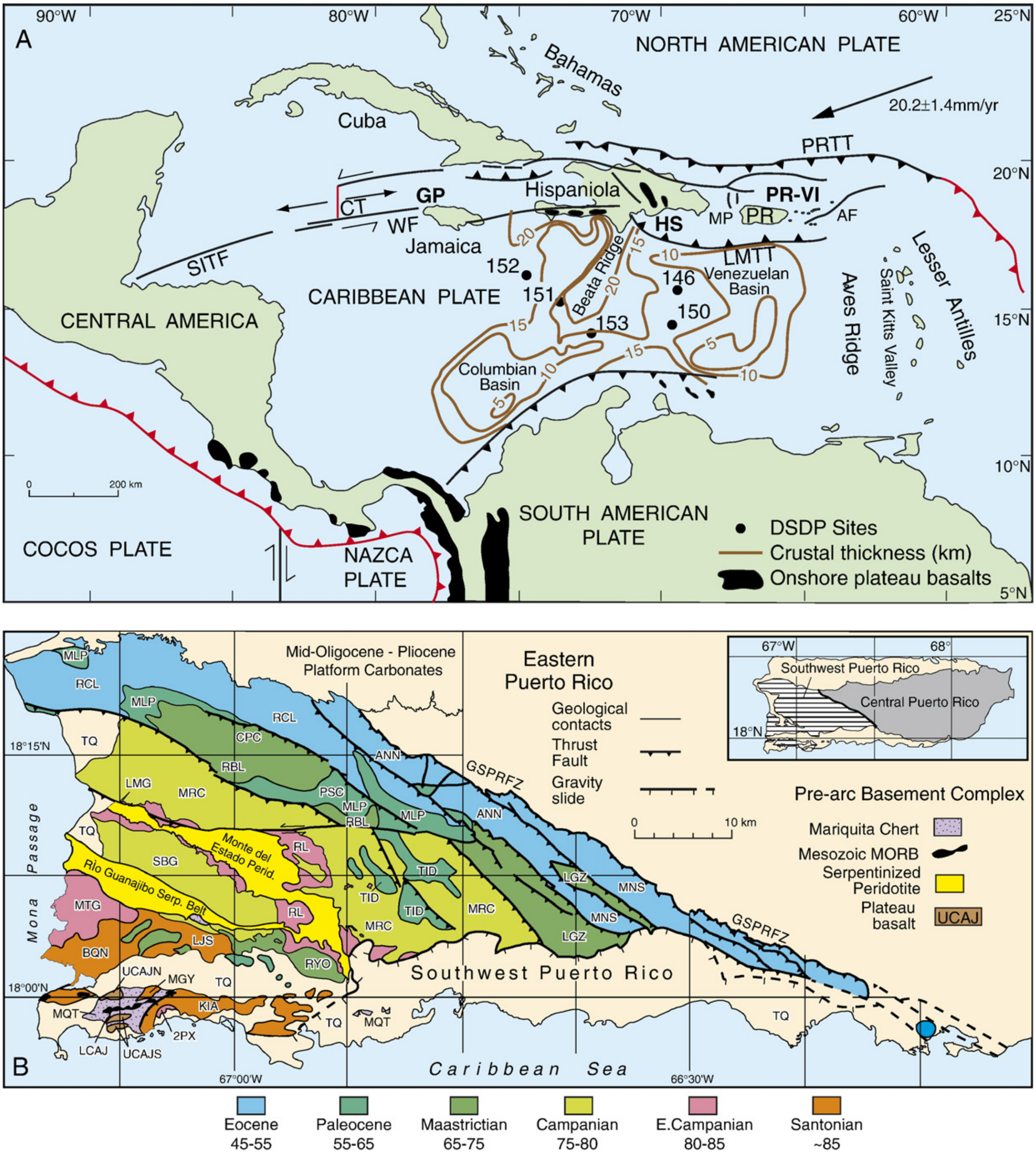

Fig. 1. (A) Map of the Caribbean region showing principal structural elements associated with the tectonic boundary between the North American and Caribbean Plates (solid lines represent fault zones, teeth represent polarity of subduction zones). The vector (Jansma et al., 2000) indicates motion of the Atlantic Basin with respect to a stable Caribbean. The locations of DSPD drilling sites within the Caribbean basalt plateau are indicated. Contours in the Caribbean Basin represent thickness (km) of oceanic crust (seismic velocity < 5.0; Pindell et al., 2006). Additional features identified as follows: AF, Anegada Fault; WF; AI, Aves Island. Exposures of on-shore Caribbean plateau basalts are from Hauff et al. (2000); CT, Cayman Trough spreading center; GP, Gonive Microplate; HS, Hispaniola microplate; LMTT, Los Muertos Trench Thrust; PR, Puerto Rico; PRTT — Puerto Rico Trench Thrust; PR-VI, Puerto Rico–Virgin Islands microplate; SITF, Swan Is. Transform Fault; WF, Walton Fault. (B) Geologic map of south western Puerto Rico, compiled from US Geological Survey sources, indicating distribution of principal stratigraphic units. Unit codes are the same as in Fig. 6 and Table 1; TQ, Quaternary–Tertiary cover. Other features mentioned in the text are identified as follows: MQT, Mariquita chert; GSPRFZ, Greater Southern Puerto Rico Fracture Zone. LCAJ represents the Lower Cajul formation tholeiitic lavas; UCAJ the Upper Cajul Formation plateau basalts, and MGY the Maguayo Stock.

2.2. Eastern Puerto Rico

Puerto Rico is dominated by an arched and deeply eroded volcanic core and ringed by predominantly shallow marine sediments of mid-Oligocene to Pliocene age (van Gestel et al., 1999; Iturralde-Vinent and McPhee, 1999). The island consists of two major tectonic blocks separated by northeast-directed high-angle thrust faults known as the Greater Southern Puerto Rico Fracture Zone (Fig. 1B; Schellekens, 1993, 1998). The predominantly east-trending volcanic strata in eastern Puerto Rico, dating between the Early Albian and mid-Eocene (115–45 Ma), contain the thickest and most extensive accumulation of strata in the island. Volcanism was relatively continuous until the Maastrichtian (~70 Ma), when it became intermittent and was largely replaced by widespread granitoid plutonism (Donnelly 1989; Schellekens, 1993; Lidiak and Jolly, 1996; Smith et al., 1998). The thickness of strata reached up to 14 km (Jolly et al., 1998), but underplating during the Maastrichtian (Smith et al., 1998) thickened the crust to approximately 30 km. In comparison, the total crustal thicknesses in southwest Puerto Rico are lower, reaching a maximum of up to 15 km (Boynton et al., 1979).

2.3. Southwestern Puerto Rico

Paleontologic assemblages (Santos, 1999) indicate that arc strata in southwest Puerto Rico decrease in age from Santonian in the far southwest to mid-Eocene (from ~85 to 45 Ma) in the northeast (Figs. 1B, 2). In addition, a K–Ar isotope age of 86.1±1.2 μa, representing the onset of arc volcanism, was reported from the Maguayo andesite stock in the Sierra Bermeja area (Fig. 1B; Schellekens, 1991). Volcanic strata in southwest Puerto Rico are most conveniently subdivided on the basis of rock types into four northwest trending volcanic belts. The southwestern-most belt, extending northward from Sierra Bermeja across the Río Guanajibo serpentinite belt to the southern border of the Monte del Estado serpentinized peridotite (Fig. 1B), is dominated by plagioclase-augite-hornblende-bearing tuff and subordinate basalt, basaltic andesite, and andesite lava (Boquerón, Lajas, Monte Grande, Sabana Grande, and El Rayo Formations; Figs. 1 and 2, Table 1). The central belt, which is concentrated along the margins of the Monte del Estado peridotite, comprises up to 1 km of high-Mg andesite lava, normally consisting predominantly of massive pillows up to 2 m in diameter (Río Loco Formation, sometimes called a two-pyroxene gabbro (Krushensky and Monroe, 1978)). Rocks of identical composition and mineralogy intrude Late

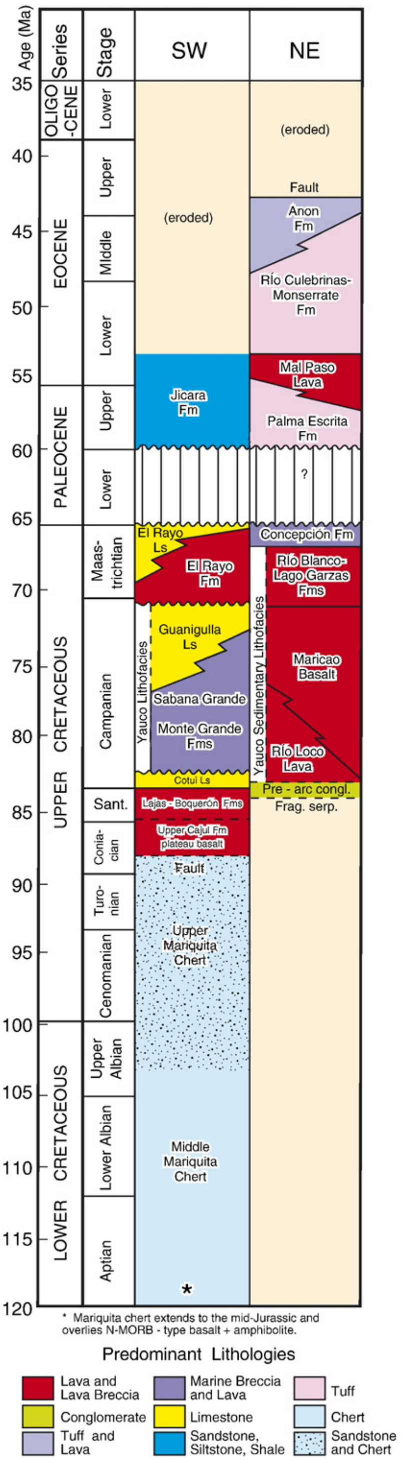

Fig. 2. Stratigraphic correlations in southwest Puerto Rico (modified from Jolly et al., 1998; Schellekens, 1998; Santos, 1999). Geologic time scale is from Gradstein et al. (2004).

Table 1
Volcanic units in southwest Puerto Rico

Code	unit name (depositional environment)	Phenocrysts
Tertiary		
11. Early through Late mid-Eocene (55 to 44 Ma)		
ANN	Anon Fm (Volcanic axis, VA)	pl, hb, ±cpx
MNS	Monserrate Fm (VA)	pl, hb, ±cpx
RCL	Río Culebrinas Fm (VA)	pl, hb, ±cpx
TID	?Tertiary intrusives (VA?)	pl, hb, ±cpx
10. Paleocene (65 to 55 Ma)		
MLP	Mal Paso Fm (Volcanic axis, VA)	pl, hb, ±cpx
PSC	Palma Escrita Fm (VA)	pl, hb, ±cpx
Late cretaceous		
9. Latest Maastrichtian (~60 to 65 Ma)		
CPC	Concepción Fm (VA)	pl, cpx, hb?
8. Maastrichtian (72 to ~60 Ma)		
RYO	El Rayo Fm (Foreaec, FA)	pl, hb, cpx
LGZ	Lago Garzas Fm (VA)	pl, cpx
RBL	Río Blanco Fm (VA)	pl, cpx
7. ?Late Campanian (?80 to 72 Ma)		
SBG	Sabana Grande Fm (FA)	pl, cpx, hb
SBG-PA	Porphyritic andesite (FA)	pl, cpx, hb
6. Campanian (?85 to 72 Ma)		
MRC	Maricao Basalt (VA)	cpx, pl, ol
5. Early Campanian (85 to 80 Ma)		
MTG	Montegrande Fm (FA)	pl, hb
4. ?Early Campanian (?85 to 80 my)		
RL	Río Loco Fm (Back forearc, FA)	cpx, opx, pl, ol?
2PX	Two-pyroxene basalt, Río Loco-like (FA?)	cpx, opx, pl, ol?
3. Santonian (~85 Ma)		
BQN	Boquerón Fm (FA)	pl, cpx, hb, ol
LJS	Lajas Fm (FA)	pl, hb, ±cpx
MGY	Maguayo andesite (FA) K–Ar=86.1±2.1 Ma	pl, hb
KIA	?Late Cretaceous intrusives (FA)	pl, hb
2. ?Santonian (>85 Ma)		
UCAJS	Upper Cajul Basalt (OIB-type basalt)	pl, cpx
UCAJN	Upper Cajul Basalt (plateau basalt)	cpx
Early to mid-Jurassic		
1. Pre-Late Pliensbachian (>195 Ma)		
LCAJ	Lower Cajul Basalt (N-MORB)	cpx, pl, ol
AMPH	Las Palmas Amphibolite (N-MORB)	hb, pl, ±cpx

VA, volcanic axis, FA, forearc.

Santonian limestone in the Sierra Bermeja area (Volckmann, 1983; Fig. 1B), indicating that the high-Mg andesites are no older than earliest Campanian (Fig. 2). A third, broader northeast volcanic belt of Campanian age consists predominantly of fine- to medium-grained volcanic sediment interlayered with (a) augite-rich basaltic volcanic breccia and porphyritic basalt lava (Maricao Basalt), and (b) pillow basalt and associated tuffaceous strata (Río Blanco and Lago Garzas Formations). Campanian basalts are succeeded by a thick sequence of intermediate hornblende-bearing Paleocene and Early Eocene tuff and subordinate lava not included in this investigation. Except possibly for a brief period during the Maastrichtian (McIntyre, 1974), eruptive activity persisted in southwestern Puerto Rico until the mid-Eocene (Schellekens, 1993, 1998), when the arc was thrust northeastward onto the adjacent arc platform in eastern Puerto Rico (Erikson et al., 1990). Accompanying high-angle faulting and isoclinal folding greatly contracted the width of the arc (Dolan et al., 1991).

Table 2
Average anhydrous compositions of SWPR lavas

Formation	U. Cajul N	Río Loco	Maricao	Boquerón	Sabana Grande	El Rayo
Code	UCAJN	RL	MRC	BQN	SBG	RYO
SiO2, wt.%	53.45	58.71	50.20	56.30	54.47	53.94
TiO2	1.93	0.75	1.14	0.82	1.01	1.02
Al2O3	16.91	12.18	15.34	17.14	17.86	18.94
FeO*	9.61	8.17	10.42	7.99	7.88	6.69
MnO	0.18	0.14	0.19	0.17	0.14	0.14
MgO	4.54	8.34	7.87	3.94	3.89	3.03
CaO	7.45	7.42	10.96	8.64	8.19	9.52
Na2O	4.44	2.38	3.05	3.35	4.32	5.00
K2O	1.26	1.62	0.63	1.30	1.04	1.30
P2O5	0.23	0.29	0.19	0.35	0.39	0.42
LOI	4.74	2.75	3.05	4.44	3.60	5.30
Cr, ppm	145	234	176	123	46	31
Ni	51	76	36	33	21	12
Co	44	35	47	29	24	24
Sc	53	27	50	26	31	24
V	53	35	36	33	21	12
Pb	6	6	5	10	19	6
Cs	1.08	0.48	0.24	0.56	1.27	0.27
Ba	204	1187	246	1012	682	810
Sr	316	570	618	715	698	810
Ba	204	1187	246	1012	682	810
Sr	316	570	618	715	698	810
Ta	0.75	0.92	0.30	0.93	0.71	0.62
Nb	10.1	14.5	4.9	12.8	11.0	10.2
Hf	3.12	2.91	1.65	3.81	3.06	3.78
Zr	111	113	52	134	111	133
Y	38	14	21	22	26	25
Th	0.99	4.16	0.81	4.10	2.97	3.29
U	0.43	1.33	0.45	1.26	1.41	1.84
La	10.26	23.55	8.08	23.11	19.97	21.63
Ce	23.51	42.01	18.87	43.76	39.07	43.89
Pr	3.33	5.07	2.78	5.57	5.28	6.02
Nd	17.58	20.40	13.31	23.18	22.82	26.93
Sm	4.55	3.96	3.52	4.52	5.07	5.83
Eu	1.68	1.02	1.11	1.36	1.49	1.57
Tb	1.06	0.44	0.62	0.66	0.71	0.70
Dy	6.30	2.39	3.50	3.91	4.33	4.10
Ho	1.33	0.46	0.75	0.76	0.87	0.81
Er	3.82	1.28	2.18	2.15	2.54	2.30
Tm	0.57	0.19	0.32	0.32	0.37	0.34
Yb	3.46	1.23	2.00	2.15	2.51	2.04
Lu	0.53	0.19	0.32	0.35	0.37	0.35

Table 3
Sr-, Nd-, and Pb-isotope data, southwestern Puerto Rico

Sample code	$^{206}Pb/^{204}Pb$	$^{207}Pb/^{204}Pb$	$^{208}Pb/^{204}Pb$	Pb, ppm	$m^{87}Sr/^{86}Sr$	Rb	Sr	$i^{87}Sr/^{86}Sr$	$m^{143}Nd/^{144}Nd$	Nd	Sm	$i^{143}Nd/^{144}Nd$	ε_{Nd}	Age, Ma
A. Pre-arc basement complex														
LCAJA	19.55	15.57	38.56	1	0.704330	2	56	0.704067	0.513040	38.00	11.70	0.512815	8.09	185
LCAJB	19.39	15.57	38.72	1	0.704500	5	103	0.704143	0.513066	36.00	10.70	0.512848	8.75	185
LCAJC	18.95	15.55	38.48	2	ND	10	100	ND	0.513070	15.26	4.88	0.512851	8.77	185
LCAJDS/103B	18.70	15.55	38.16	1	0.704486	13	261	0.704119	0.513043	7.31	2.70	0.512773	7.27	185
LCAJE	19.97	15.56	39.01	2	0.704450	5	74	0.703953	0.513046	36.72	10.30	0.512841	8.60	185
UCAJN103C	18.85	15.65	38.50	2	0.705220	24	266	0.704921	0.512925	12.82	3.31	0.512843	6.13	85
UCAJN103D	19.24	15.57	39.05	2	0.704910	35	303	0.704520	0.512921	20.56	5.41	0.512832	5.72	85
UCAJN103G	19.25	15.59	38.90	11	0.704950	30	402	0.705250	0.513047	15.77	3.73	0.512923	6.73	85
UCAJN103A	19.29	15.60	39.18	2	0.705010	22	249	0.703920	0.512985	12.70	3.10	0.512910	6.54	85
UCAJS303/S3	21.15	15.65	40.43	5	0.704640	8	270	0.704495	0.512823	46.31	9.76	0.512750	4.79	85
UCAJS303/S5	21.01	15.67	40.51	5	0.705010	19	488	0.703920	0.512985	44.32	8.08	0.512910	6.54	85
B. Santonian to Maastrichtian high-Mg andesites and related lavas														
ANN54–94	18.82	15.59	38.50	3	0.704800	16	480	0.704734	0.512956	14.16	2.94	0.512915	6.66	50
ANN/VP159 [a]	18.80	15.61	38.49		0.704010	38	537	0.703870	0.512877	23.94	4.54	0.512838	5.17	50
ANN/VP176 [a]	18.85	15.64	38.62		0.704030	15	426	0.703960	0.512769	17.48	3.78	0.512726	2.98	50
BQN103/9.8A	18.95	15.59	38.70	3	0.704100	2	399	0.704083	0.512874	21.72	4.10	0.512811	5.50	85
BQN300/1.2D	19.09	15.60	38.73	3	0.703940	41	670	0.703733	0.512928	21.81	4.22	0.512863	6.52	85
CPC124/1.0	18.63	15.55	38.16	4	0.703690	15	493	0.703605	0.512996	11.22	2.70	0.512929	7.44	70
MLP105/42.5	18.84	15.62	38.48	5	0.703990	10	359	0.703925	0.512985	15.54	3.52	0.512936	7.19	55
MLP409/6.5	18.79	15.59	38.47	8	0.705550	12	318	0.705418	0.512983	21.01	5.82	0.512923	6.94	55
MLP/EC5 [a]	18.91	15.64	38.61	6	0.704070	8	433	0.704033	0.512953	13.05	3.32	0.512903	6.42	50
MNS2/167.0C	18.77	15.55	38.33	10	0.704060	4	883	0.704050	0.512927	26.62	5.41	0.512887	6.11	50
MRC120/23	19.64	15.54	38.17	1	0.703700	9	514	0.703648	0.512994	14.91	2.92	0.512936	7.70	75
MTG395/1.5B	18.88	15.65	38.60	29	0.704280	26	549	0.704129	0.512828	32.07	7.29	0.512756	4.31	80
RBL124/10.1	18.66	15.56	38.21	8	0.703800	24	564	0.703682	0.512975	14.99	3.48	0.512911	7.08	70
RCL/CF1a [a]	18.78	15.63	38.49		0.704740		349	0.704670	0.512954	14.39	3.43	0.512907	6.50	50
RL356.6/3.65	19.08	15.62	38.81	5	0.704980	55	710	0.704980	0.512794	22.72	4.69	0.512729	3.78	80
RLR-93	18.89	15.65	38.61	2	0.704030	27	1851	0.703987	0.512764	21.74	4.99	0.512696	3.01	75
RYO328/5.1	18.85	15.62	38.50	4	0.703920	19	821	0.703855	0.512936	26.23	6.53	0.512867	6.23	70
RYO332/6.2	18.85	15.56	38.32	5	0.705200	3	8090	0.705199	0.512993	21.70	4.11	0.512941	7.66	70
C. Toa Baja drill core, eastern Puerto Rico														
TOA2134 [a]	18.67	15.63	38.41		0.705800	28	537	0.705696	0.512737	8.64	2.4	0.512682	2.11	50
TOA2149 [a]	18.68	15.63	38.42		0.706040	28	426	0.705909	0.512606	8.28	2.29	0.512551	−0.45	50
TOA3115 [a]	18.79	15.58	38.35		0.704000	2.7	243	0.703980	0.512987	27.86	7.45	0.512934	7.02	50

[a] Data from Frost and Schellekens (1998).

3. Analytical procedures

Sample preparation was performed in mullite vessels to insure minimal trace element contamination. Complete major (ICP-ES) and trace element (ICP-MS) analyses of 278 rocks were performed for this project by Acme Analytical Laboratories at Vancouver, BC, utilizing $LiBO_2$ fusion techniques. Duplicate analyses and deviations from geochemical standard curves reveal precision is within 1 to 5% of the amount present or better for most trace elements. A total of 99 analyses are presented in On-line Tables OL1B and OL2B in Appendix A, including (1) 7 samples from Deep Sea Drilling Project (DSDP) drill-cores representing the Caribbean basalt plateau in the central Caribbean Basin (locations shown in Fig. 1A); (2) 18 Caribbean plateau basalts from the Upper Cajul Formation (Fig. 1B) in southwest Puerto Rico; (3) 73 island arc lavas, including 11 Boquerón, 18 Río Loco, 11 Sabana Grande, 11 Maricao, 8 El Rayo, and 15 Río Blanco–Lago Garzas samples (Fig. 1B). Representative lava clasts from coarse-grained tuffaceous strata were sampled when suitable lava flows were unavailable. A key to sample numbers and sample locations are given in On-line Tables OL1A and OL2A in Appendix A, and average compositions of major stratigraphic units are listed in Table 2.

Sr- and Nd-isotope analyses (Table 3) were performed utilizing dynamic multiple collection on a VG Isolab 54T machine at McMaster University. Analysis of the NBS 987 Sr standard (normalized to $^{86}Sr/^{88}Sr = 0.1194$) during the course of this work yielded an average $^{87}Sr/^{86}Sr$ value of 0.710251 ± 0.000024 (2σ). The average within-run precision on Sr standards and samples was 0.0024% (2σ). Analysis of the La Jolla Nd standard (normalized to $146/144 = 0.729$) yielded an average $^{143}Nd/^{144}Nd$ value of 0.511862 ± 0.000015 (2σ), with average within-run precision of 0.0026% (2σ). Nd analyses are quoted relative to a value of 0.51185 for La Jolla. Duplicate Sr-isotope analyses were made of samples treated by strong hot acid leaching according to the following procedures: the samples were leached in hot 3 m HCl overnight, washed, and treated again overnight by leaching in a cold acid solution of HF, HCl, and HNO_3; a comparison of the two sets revealed minimal differences (Jolly et al., 2001).

Pb was separated in 0.2 ml exchange columns using HBr. After loading on Re filaments, using silica gel and H_3PO_4, Pb was analyzed on a VG354 spectrometer with a Faraday collector at McMaster University. Pb-isotope data (Table 3) are corrected for mass fractionation of 0.08% per atomic mass unit (amu), based on analyses of the NBS 981 standard. Estimated 2σ reproducibility, based on standard analyses and replicate analysis of samples, is as follows: $^{206}Pb/^{204}Pb$, (± 0.020; $^{207}Pb/^{204}Pb, \pm 0.015$; $^{208}Pb/^{204}Pb, \pm 0.040$. Data are not corrected for radiogenic Pb growth since eruption, because the magnitude of this small effect is expected to be similar to radiogenic growth of mantle reference sources over the same time period.

4. Major and trace element geochemistry

Sub-greenschist grade alteration of Cretaceous volcanic strata in southwest Puerto Rico is normally characterized by extensive chloritization (hydration) of groundmasses and hornblende crystals, albitization of feldspar, and serpentinization of olivine and orthopyroxene phenocrysts. In addition, zeolites, prehnite, and more rarely pumpellyite and epidote, are present sporadically as void filling secondary minerals. Despite the extensive alteration, relict minerals are abundant in most samples, commonly as isolated domains within phenocryst cores. Since secondary minerals do not extend across original grain boundaries, relict textures are well preserved in virtually all samples. Penetratively deformed actinolite-epidote-albite-bearing greenschists, restricted largely to the vicinity of intrusive bodies, were excluded during sample selection.

Although considerable care was taken to select the least altered samples for analysis, several limitations arise from the pervasive low-temperature alteration. Most significantly, the mobilization of water-soluble elements produced dispersed geochemical distribution patterns, masking any slab-derived aqueous component contributed by metasomatizing fluids, and rendering problematic both normative compositions and rock classifications based on abundance of mobile K_2O (Peccerilo and Taylor, 1976; La Maitre, 1989). Consequently, this study is restricted to major and trace element components that are stable in the presence of chloride brines, including high field strength elements (HFSE), rare earth elements (REE), and Th (Pearce and Parkinson, 1993). Large-ion lithophile elements (LILE; Rb, Cs, Ba, U, K, Sr) are excluded. Apart from the alkali elements, major element oxides form tight fields when plotted against more immobile components, such as Al_2O_3, indicating that their measured abundances reflect original compositions. To minimize scatter introduced by hydration, data in diagrams and models were recalculated on an anhydrous basis to 100%. Volcanic classes, based on SiO_2 abundance (Peccerillo and Taylor, 1976), include basalt ($SiO_2 = 45–53\%$), basaltic andesite, (53–57), andesite (57–63) dacite (63–70), and rhyolite (<70). Units that contain a range of compositions are characterized for convenience by the dominant class represented. The spectrum of volcanic rocks is subdivided utilizing SiO2 vs FeO*/Mg relations (FeO* represents total Fe calculated as FeO) into high-, medium-, and low-Fe suites according to the method of Arculus (2003), which compliments divisions of relatively unaltered Cenozoic suites based on K_2O content (Gill, 1981).

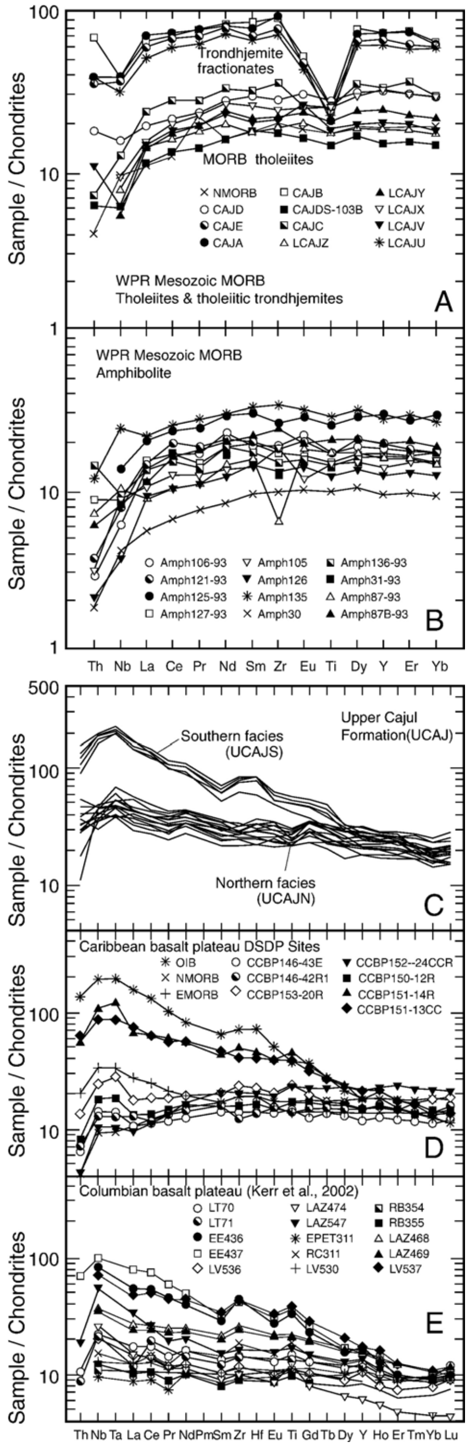

Fig. 3. Chondrite normalized incompatible trace element patterns for (A) MORB tholeiites and trondhjemitic fractionates from the Lower Cajul Formation (Jolly and Lidiak, 2006) and (B) Las Palmas Amphibolites, both from the pre-arc Sierra Bermeja Complex in southwest Puerto Rico; (C) Upper Cajul Formation plateau basalts (UCAJ), subdivided into northern (N) and southern (S) facies (Fig. 1C); (D) Central Caribbean basalt plateau (DSDP sites 146–153; additional analyses are provided by Kerr et al., 2002); (E) Columbian basalt plateau (Kerr et al., 2002). Chondrite composition and order of elements are from Sun and McDonough (1989).

4.1. Pre-arc basement

4.1.1. Jurassic N-MORB-type tholeiites

Tholeiitic lavas (LCAJ) and amphibolites from the basement complex, representing remnants of Jurassic MORB (Schellekens et al., 1990; Schellekens, 1991; Jolly et al., 1998) from the Mesozoic Farallon (proto-Pacific) Plate (Montgomery et al., 1994), have depleted normalized incompatible element patterns (Fig. 3A and B) characterized by low La/Nb and La/Sm (averaging 0.90 and 1.20 respectively, Jolly et al., 1998), similar to N-MORB. The rocks have N-MORB-like ε_{Nd}-values (average approximately 9.0) and initial (i) $^{87}Sr/^{86}Sr$ (average 0.7038; Jolly et al., 2001), overlapping modern Atlantic MORB (Dosso et al., 1993). Tholeiite lavas are interlayered with trondhjemitic fractionates (Jolly and Lidiak, 2006) and are associated with amphibolites, representing layered gabbroic intrusives. Hornblende from amphibolites yielded maximum K–Ar ages of 126 ± 3 Ma (Cox et al., 1977), considered a metamorphic age imposed by an early magmatic event also recognized in the Duarte basement complex in Hispaniola (Lapierre et al., 1999; Lewis et al., 2002).

4.1.2. Late Cretaceous plateau basalts

The uppermost basement unit in the pre-arc sequence comprises two distinct geographic facies of plateau basalt from the Upper Cajul Formation (UCAJ), both of which consist of fine-grained, incompatible element-enriched basaltic lava flows with sparse plagioclase phenocrysts. The contacts between the lavas and underlying chert are not exposed, but relative stratigraphic positions indicate that basalts from the Upper Cajul Formation were erupted late in the pre-arc sequence. The northern facies (UCAJN) is preserved as fault blocks within the Mariquita Chert on the north flank of Sierra Bermeja (Fig. 1B), whereas the more enriched southern variant (UCAJS) is interlayered with pelagic chert on the south flank (Volckmann, 1983). The units represent local facies of the Late Cretaceous Caribbean basalt plateau, the major eruptive phase of which is dated between 92 and 83 Ma (Lapierre et al., 1997, 1999; Révillon et al., 2000;

Kerr et al., 2002; Kerr and Tarney, 2005). Samples from the northern facies (UCAJN, Table 2 and On-line Table OL2B, Appendix A) have from 49 to 56% SiO_2 (Fig. 4), 14 to18% Al_2O_3, and 4 to 6% MgO. Normalized incompatible element patterns overlap E-MORB, although there is a slight deficiency in Yb (Fig. 3C). Low La/Nd, La/Sm, and Nb/Yb indicate that the lavas represent evolved variants of more depleted Columbian types from Groups 3 and 4 of Kerr et al. (2002), which were generated by 15 to 20% melting of garnet-bearing spinel peridotite. In comparison, the southern facies (UCAJS) has high Th, LREE, and HFSE, resembling Columbian plateau basalts from Groups 1 and 2, which were generated by 3–5% melting of enriched garnet-spinel peridotite.

4.2. Island arc strata

4.2.1. Petrography

Lavas from southwest Puerto Rico are predominantly porphyritic (Table 1), although the less siliceous samples from most units tend to be aphyric or relatively phenocryst-poor and therefore more closely represent melt compositions. Many samples contain as much as 20% phenocrysts. Plagioclase and augite, up to a 0.5 cm in length, are present in all units, but rocks from the southwestern volcanic belt contain in addition brown hornblende (up to 5%), while representatives from the central belt contain ubiquitous low-Fe orthopyroxene (<5%). Samples from the central and northeastern belts are normally clouded with abundant, commonly sub-trachytic, plagioclase microlites measuring <0.5 mm in length. Plagioclase and augite are typically the most abundant phenocryst phase in hornblende-bearing rocks from the southwestern belt, whereas a combination of tiny euhearal enstatite crystals, averaging about 0.2–0.5 mm in diameter, and Fe-rich augites, up to 0.5 cm in diameter, characterize high-Mg andesite samples from the central belt. Large glomeroporphyritic augite clusters, up to 1 cm in diameter, are characteristic in basalts from the northeastern belt. The abundance of plagioclase in all the rocks is consistent with varying degrees of low-pressure subvolcanic fractional crystallization. Groundmasses of most samples consist of feathery to spherulitic devitrified glass that incorporates small proportions of magnetite and apatite. Groundmasses of many samples of high-Mg andesite pillow lava have granular or diabasic texture.

4.2.2. Southwest volcanic belt

Fields of hornblende-bearing basalts and andesites from the southwest belt (Figs. 4A–D; 5A–C) plot within the moderate-Fe field of Arculus (2003) on SiO_2 vs FeO*/MgO diagrams. As a result, the lavas cluster along the boundary between the calc-alkaline and tholeiitic series of Miyashiro (1974), although the fields are slightly off-set toward tholeiites (Fig. 5A). The average SiO_2 content of individual lava units declines slightly from a maximum of approximately 56% in early Boqueròn lavas, to almost 55% in the Sabana Grande Formation, and finally to 54%

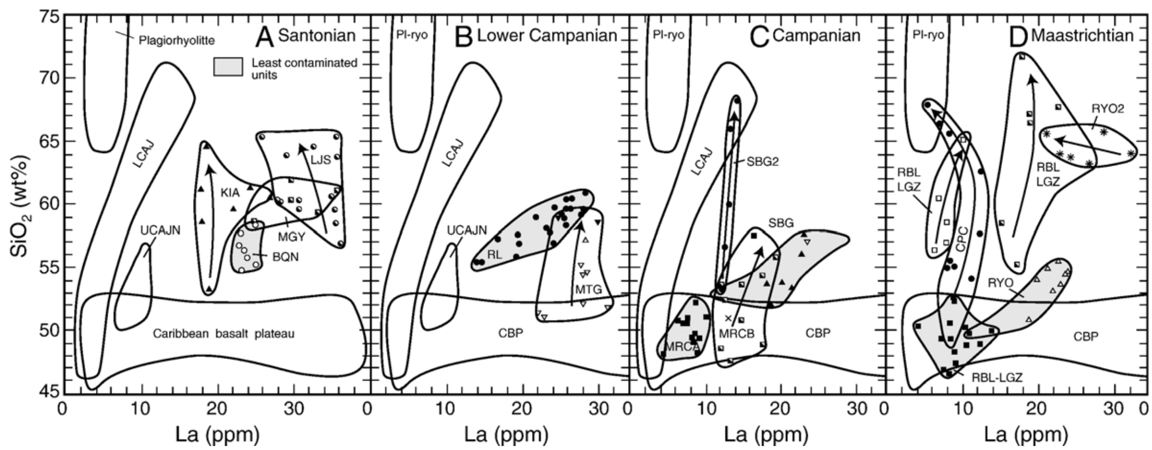

Fig. 4. Covariation of SiO_2 (wt.%) and La (ppm) in lavas from southwest Puerto Rico. Increasing SiO_2 in hybrid units is indicated by arrows; least contaminated units, which are emphasized in this report, are shaded. (A) Santonian (~85 Ma, Schellekens, 1991), including the Maguayo Stock (MGY), Cretaceous intrusive andesite (KIA), Boquerón (BQN) and Lajas Formations (LJS). (B) Earliest Campanian (~80 Ma), including the Río Loco Formation (RL, high-Mg andesite) of Slodowski (1956) and Mattson (1960) and the Monte Grande Formation (MTG). (C) Campanian (82–70 Ma), including the Sabana Grande (SBG and SBG2), and Maricao (MRCA and MRCB) Basalt. (D) Maastrichtian (70–65 Ma), including El Rayo (RYO and RYO2), Río Blanco–Lago Garzas (RBL-LGZ, 2, and 3), and Concepcíon (CPC) Formations. Also included are fields of Caribbean plateau basalts, pre-arc MORB and plateau basalts (LCAJ and UCAJ), and the eastern Puerto Rico low-pressure plagiorhyolite suite (Jolly and Lidiak, 2006).

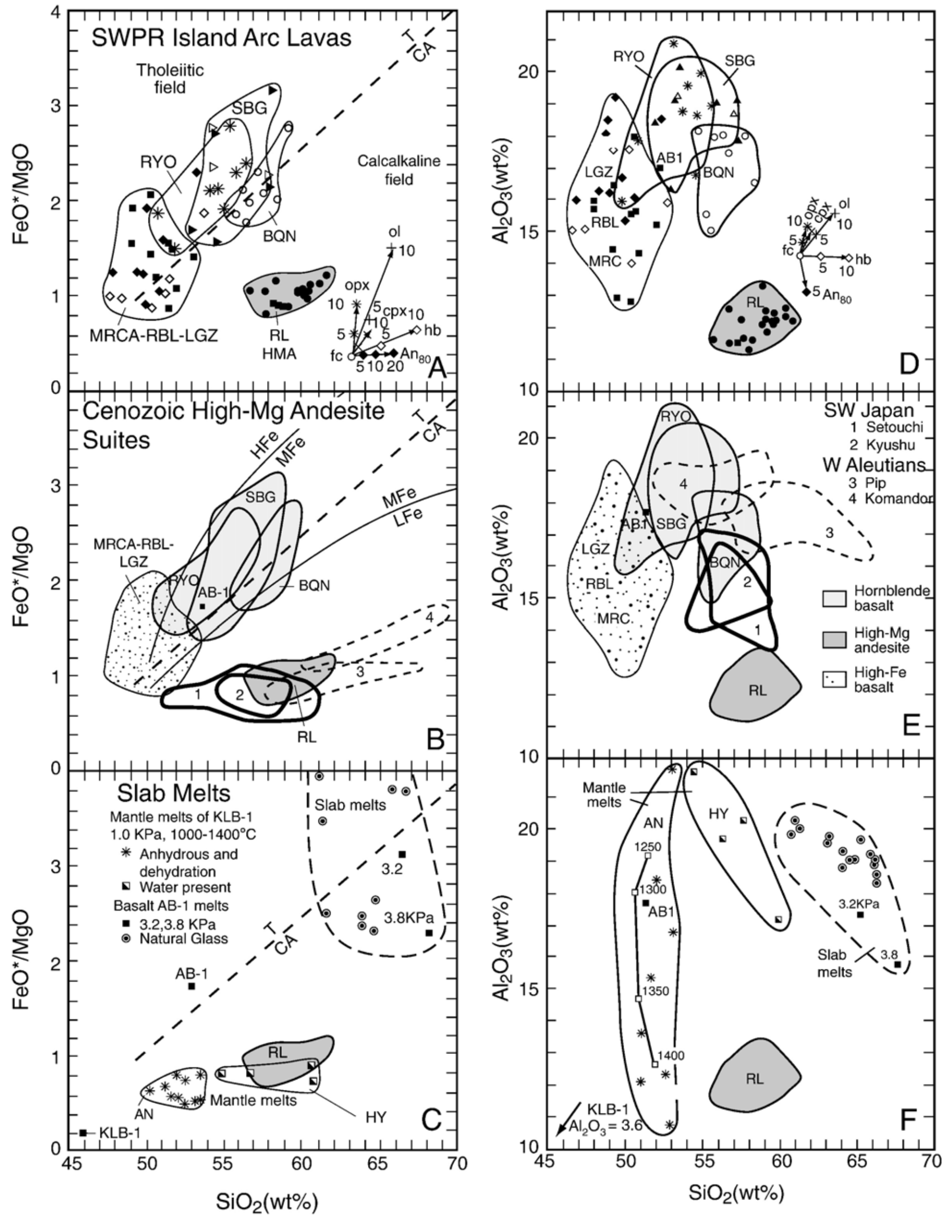

Fig. 5. Covariation of SiO_2 with FeO*/MgO (A–C) and Al_2O_3 (D–F). In A and D fields of southwest Puerto Rican lavas are outlined, whereas in B and E, the field of Puerto Rican high-Mg andesites are compared with Cenozoic high-Mg-bearing suites from southwest Japan and the western Aleutians (references are given in the text). Also indicated are fractional crystallization (fc) vectors for olivine (ol), orthopyroxene (opx), clinopyroxene (cpx), pargasitic amphibole (hb), and plagioclase (An_{80}), determined from the average Río Loco high-Mg andesite composition. In C and F the fields of anyhrous-dehydration melts and water-present mantle melts (from fusion of KLB-1 at 1100°C and 1.0 GPa, Hirose, 1997 and references therein) are compared with Río Loco high-Mg andesite and Cenozoic slab melts. Experimental melts (Rapp et al., 1999) of amphibolite basalt (AB-1) at 3.2 and 3.8 GPa and 1100°C, field of glass veins representing slab melts from Cenozoic settings (Schiano et al., 1995), are indicated.

in younger the El Rayo Formation (Figs. 4A–D, 5; Online Table OL1B, Appendix A). SiO_2 has positive correlations with FeO*/MgO, Al_2O_3 (Fig. 5A, D) and the more incompatible elements such as La and Nb (Fig. 6A and C), but broadly negative correlations with MgO, CaO, and compatible trace elements such as Ni (Fig. 6D). The rocks have high Al_2O_3 (from 15 to 21%, Fig. 5D) and Yb (2–3 ppm, Fig. 6B) compared with associated high-Mg andesites (ranging between 11 and 13% and ∼1 ppm, respectively). Chondrite normalized

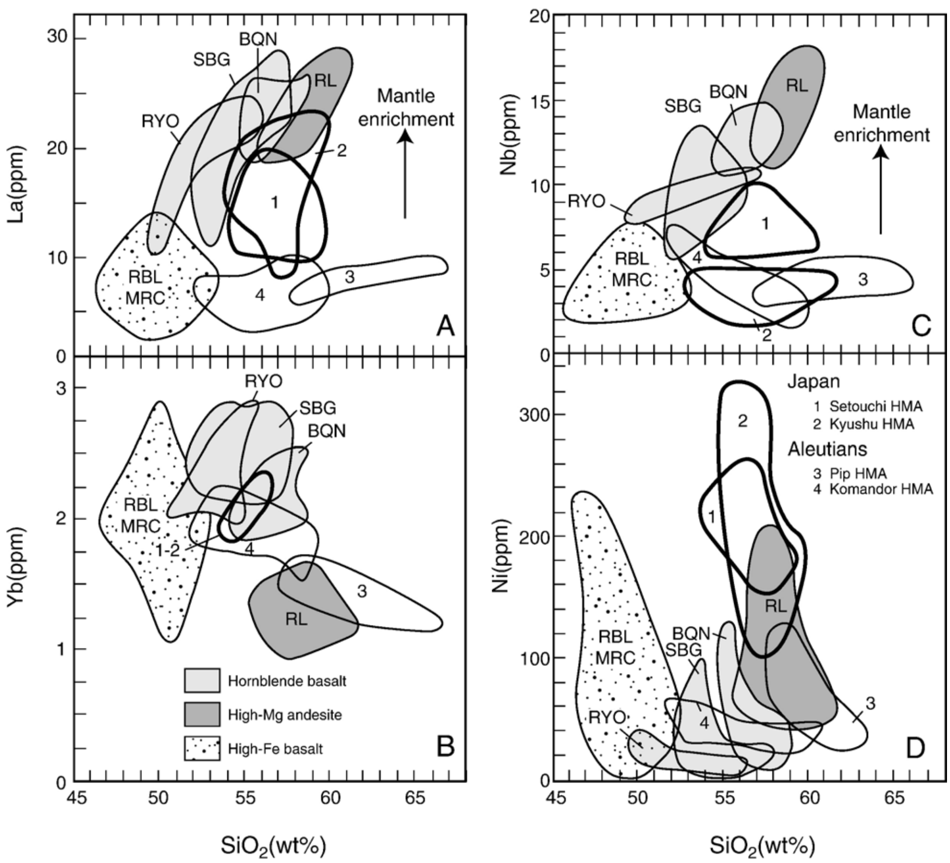

Fig. 6. Abundances of selected trace elements and SiO_2 in southwest Puerto Rico lavas compared with Cenozoic high-Mg andesite-bearing suites. (A) La, (B)Yb, (C) Nb, (D) Ni; Fields of MORB tholeiites (LCAJ) and plateau basalts (UCAJ) from southwest Puerto Rico are indicated. Also included for reference are fields from Cenozoic high-Mg bearing suites in southwest Japan and the western Aleutians.

incompatible element patterns (Fig. 7) are relatively steep with flat to faintly bowl-shaped HREE segments. REE slopes are lower in younger units, reflecting constant HREE but gradually decreasing LREE. The relative magnitudes of negative Nb- and Zr-anomalies increase in younger lavas.

4.2.3. Central volcanic belt

High-Mg andesites from the Río Loco Formation cluster within an isolated field on major element variation diagrams (Fig. 5). The rocks have elevated SiO_2/MgO (11 compared with an average of approximately 9.0 in hornblende-bearing lavas), high SiO_2 (anhydrous totals from 55 to 62%, On-line Table OL1B, Appendix A) and MgO (6.5 to 11%), but low Al_2O_3 (11 to 13.5%). Like Cenozoic counterparts (Fig. 5B and E), high-Mg andesites plot within the low-Fe field of Arculus (2003) and the calc-alkaline field of Miyashiro (1974) in SiO_2 vs FeO*/MgO diagrams. Cenozoic high-Mg andesite, restricted to between 55 and 60% SiO_2, form a broad vertical band on SiO_2-Al_2O_3 plots (Fig. 5E) of which Río Loco high-Mg andesites (11 to 21% Al_2O_3) represent the most alumina-depleted end-member. Normally, low Al_2O_3 is a hallmark of low-pressure plagiorhyolites and peralkaline rhyolites, but a mantle origin for parental melts of high-Mg andesites is indicated by elevated MgO and Ni (up to 200 ppm; Fig. 7D). Normalized patterns are similar to hornblende-bearing lavas (Fig. 7B and H), and the two suites have almost identical La concentrations (Fig. 7A), shallow negative Nb-Ta-Ti-anomalies and slight positive Zr-anomalies.

4.2.4. Northeast volcanic belt

Basalts from the northeast volcanic belt, which have from 47 to 52% SiO_2, 12 to 19% Al_2O_3, and 6 to 12% MgO (On-line Table OL1B, Appendix A), partly overlap the fields of anhydrous experimental melts (Fig. 5C and F). The rocks plot within the high-Fe field of Arculus (2003) and the calc-alkaline field of Miyashiro (1974) on SiO_2 vs FeO*/MgO diagrams (Fig. 5C and G). A small proportion

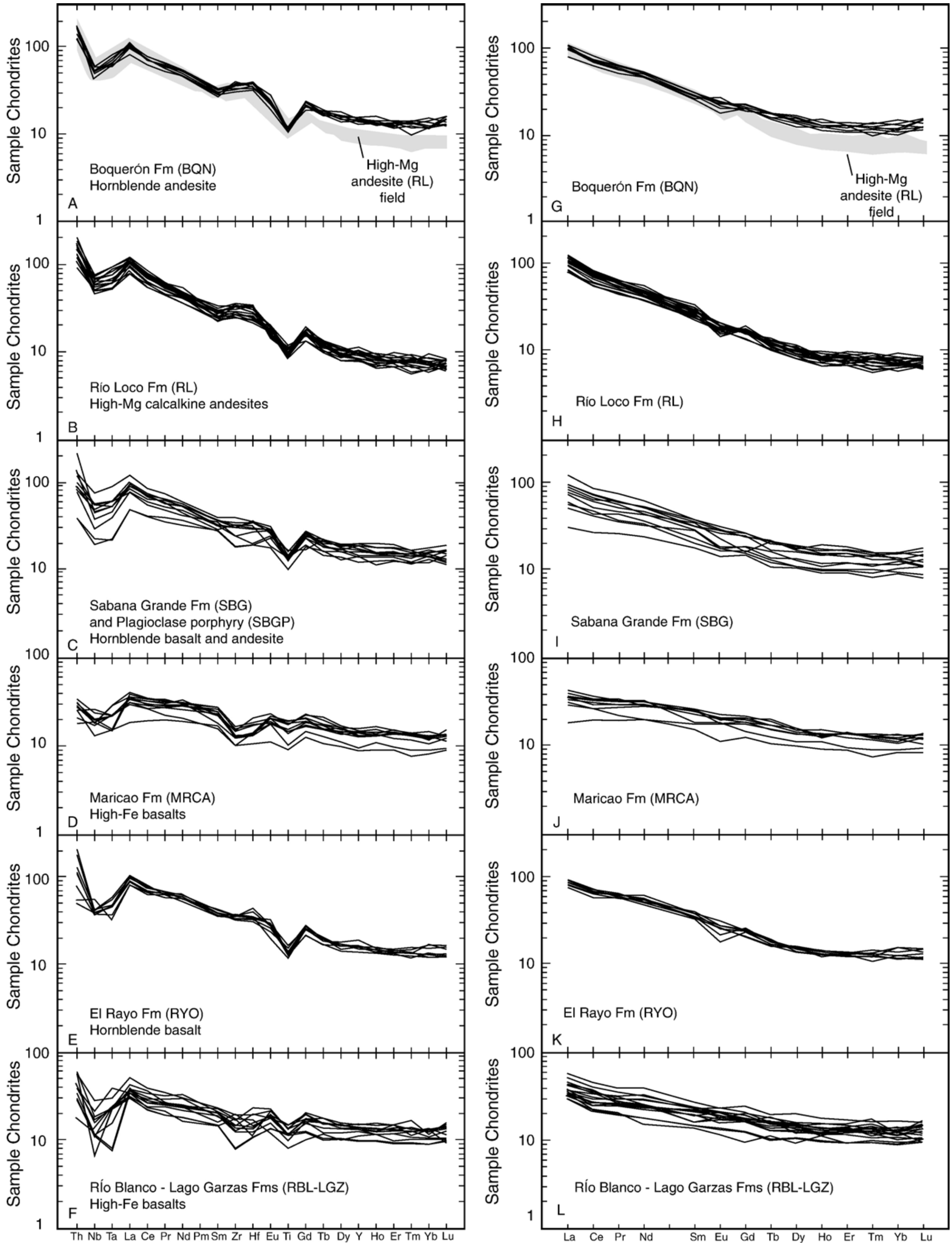

Fig. 7. Chondrite normalized incompatible element (A–L) patterns in high-Mg andesites and related lavas; normalization procedures are as in Fig. 3. In (A) the field of Río Loco high-Mg andesite is compared with the Boquerón Formation.

of the high-MgO end-members resemble high-Mg basalts (On-line Table OL1B, Appendix A), which, according to the definition of Draper and Johnston (1992), contains 9 to ~12% MgO, 15 to 16% Al_2O_3, ~10 to 2.5% CaO, and about 0.75% TiO_2. Normalized REE patterns of high-Fe basalts are generally subparallel to E-MORB, but samples from the Maricao Basalt are distinguished by a relatively shallow negative Nb-Ti-anomalies, well-developed negative Zr-anomalies, and slightly flattened LREE segments (Fig. 7C) compared with associated high-Mg andesites and related lavas. Samples from the succeeding Río Blanco and Lago Garzas Formations have more enriched LREE slopes, deeper negative HFSE-anomalies, and higher La/Nb. High-Fe basalts tend to have lower absolute incompatible element abundances and La/Yb, but higher compatible element concentrations (up to 250 ppm Ni; Fig. 6D) relative to high-Mg andesites.

5. Pb-, Sr-, Nd-isotope geochemistry

5.1. Pre-arc basement

Sr-isotope ratios in tholeiites from the Lower Cajul Formation and associated amphibolites are off-set toward sea water with respect to the mantle array (Fig. 8A and B; Table 3), consistent with the sea-floor origin. Amphibolites, with 0_{Nd} ranging between 8 and12 and $i^{87}Sr/^{86}Sr$ between approximately 0.7030 and 0.7045, are significantly less radiogenic than tholeiites, which have ranges of 8 to 9 and 0.7040 and 0.7042, respectively. In comparison, plateau basalts from the Upper Cajul Formation are more radiogenic, with lower 0_{Nd} (4 to 8), and higher $i^{87}Sr/^{86}Sr$ (0.7038 to 0.7050). As a group Puerto Rican plateau basalts have a smaller range of 0_{Nd} compared with leached samples from Columbia, but have significantly higher $i^{87}Sr/^{86}Sr$, reflecting a sea-floor alteration signature in these unleached samples. Fields of Puerto Rican tholeiites and plateau basalts are diagonal to the reference line in $^{206}Pb/^{204}Pb$ vs $^{207}Pb/^{204}Pb$ and $^{208}Pb/^{204}Pb$ plots (Fig. 8). Tholeiites approach the depleted mantle value (DM, Hart, 1984), whereas plateau basalts from both Puerto Rico and Columbia have elevated $^{208}Pb/^{204}Pb$ and $^{208}Pb/^{204}Pb$ with respect to the reference line (Hart, 1984). Samples from the northern Puerto Rican facies (UCAJN in Fig. 8) overlap Columbian basalts, with relatively low $^{206}Pb/^{204}Pb$ (18.8 to 19.6), whereas the southern facies (UCAJS) has higher values (>21).

5.2. Island arc strata

Sr–Nd isotope data from southwest Puerto Rico form an "L"-shaped field (shaded in Fig. 8C) in which high-Mg andesites and associated hornblende-bearing lavas are considerably more radiogenic than high-Fe basalt. The vertical component, with average $i^{87}Sr/^{86}Sr$ of 0.7040 and ε_{Nd} between 3 and 7, extends toward the primitive mantle value (PM, Sun and McDonough, 1989). The field is subparallel to that of leached Columbian basalts (Fig. 8B), but is slightly off-set toward higher $i^{87}Sr/^{86}Sr$, consistent with limited sea-floor alteration. The horizontal field, consisting of younger Maastrichtian and Eocene rocks, has ε_{Nd} averaging 6–7 and $i^{87}Sr/^{86}Sr=0.7040$ to 0.7055, consistent with sea-floor alteration. In comparison, the diagonal field of lavas from eastern Puerto Rico is subparallel to a calculated mixing line between pelagic sediments and an arc basalt (Jolly et al., 2001, 2006). The trend is consistent with the presence of 3 to 5% sediment, whereas the two diverging trends in southwest Puerto Rico are inconsistent with such a large pelagic sediment component.

Pb-isotope ratios in southwest Puerto Rico arc lavas (Fig. 5F and G) form well defined elongate fields extending from the Upper Cajul Formation (UCAJN) toward more depleted end-members of the tholeiitic basement suite (LCAJ), the field of which intersects the reference line above the depleted mantle value (DM; $^{206}Pb/^{204}Pb=18.4$, Hart, 1984). High-Fe basalts are the least, and high-Mg andesites the most, radiogenic. Incompatible trace element abundances (Fig. 9A–H) have strong positive correlations with isotope ratios, indicating a mixing process in which high proportions of both incompatible elements and radiogenic isotopes were contributed by a common, enriched component. The larger range of ε_{Nd} compared with Pb-isotope ratios is consistent with introduction of an excess of water soluble Pb, compared with highly insoluble Nd, by aqueous fluids emanating from the relatively less radiogenic N-MORB-type oceanic crust comprising the dehydrating lower slab (see Ellam and Hawkesworth, 1988; Arculus, 1994).

6. Petrogenesis of high-Mg andesites and related lavas

6.1. Cenozoic high-Mg andesite suites

High-Mg andesites, characterized (Tatsumi, 2001) by high-MgO (>5%), low FeO*/MgO (<1.5), Al_2O_3 (<16%), and CaO (<10%), can be generated by at least two contrasting processes. First, experimental evidence indicates that such melts are produced directly by partial fusion of hydrous peridotite (Kushiro, 1974; Mysen and Boettcher, 1975; Tatsumi, 1981; Hirose, 1997). This process, which reflects expansion of the

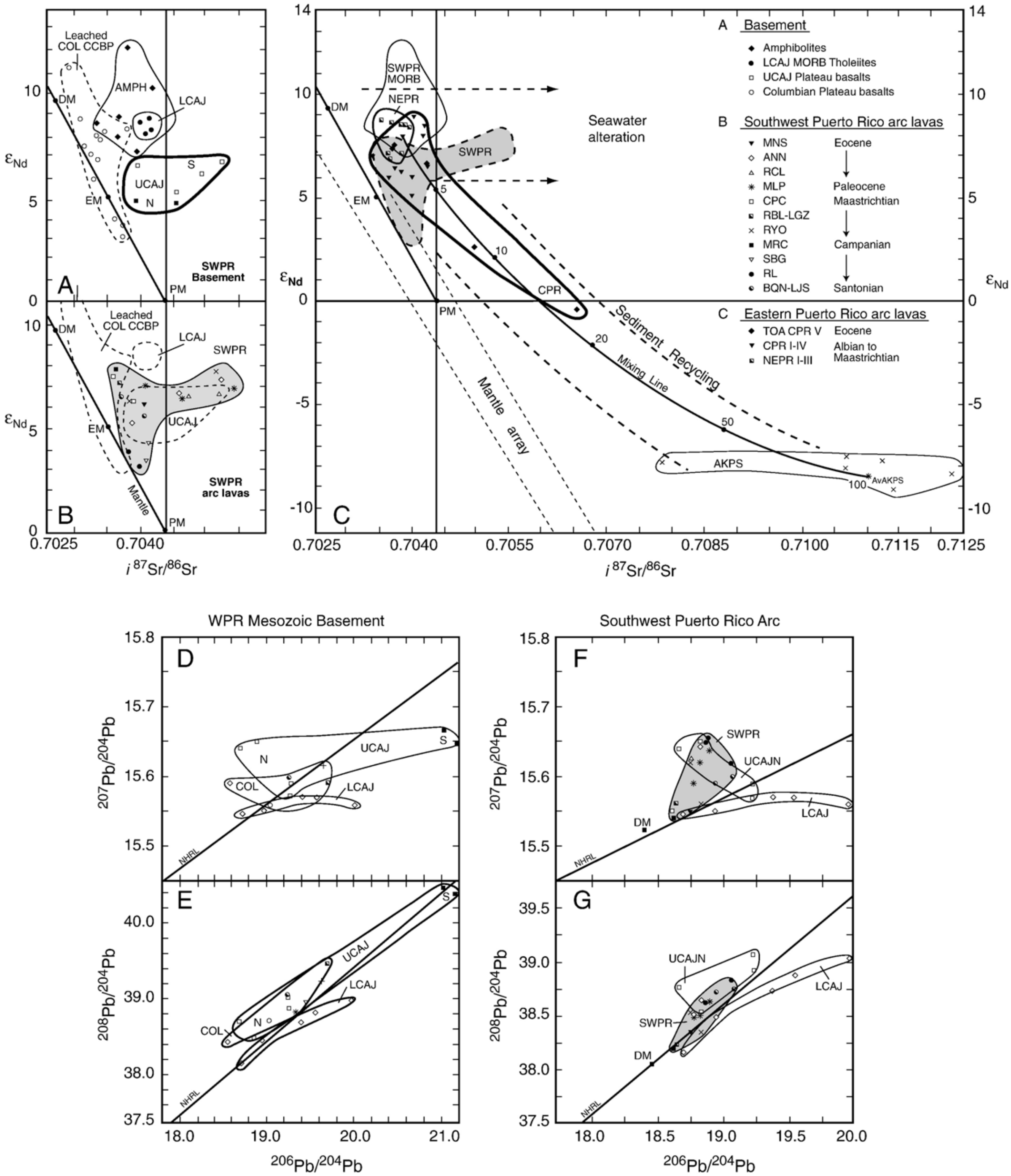

Fig. 8. Sr-, Nd-, and Pb-isotope ratios in southeast Puerto Rico (southwest Puerto Rico); mantle features are modified from Rollinson (1998). Unit codes as in Fig. 6. (A) Pre-arc basement complex, including MORB tholeiite basalts from the Jurassic Lower Cajul Formation (LCAJ), related amphibolite (AMPH), and plateau basalts from the Upper Cajul Formation (UCAJ), subdivided into northern (N) and southern (S) facies. Also included for reference is the field of leached Columbian basalts (data from Kerr et al., 2002). (B) High-Mg andesite and hornblende-bearing lavas from southwest Puerto Rico are compared with the Cajul Formation and Columbian plateau basalts. (C) Fields of southwest Puerto Rico arc lavas and MORB tholeiites are compared with island arc lavas from eastern Puerto Rico. (D and E) Pre-arc basement rocks, including Jurassic MORB (LCAJ) and plateau basalts (UCAJ) from the Cajul Formation, are compared with Columbian plateau basalts. (F and G) Pb-isotope ratios in high-Mg andesite and related lavas are compared with basement tholeiites (LCAJ).

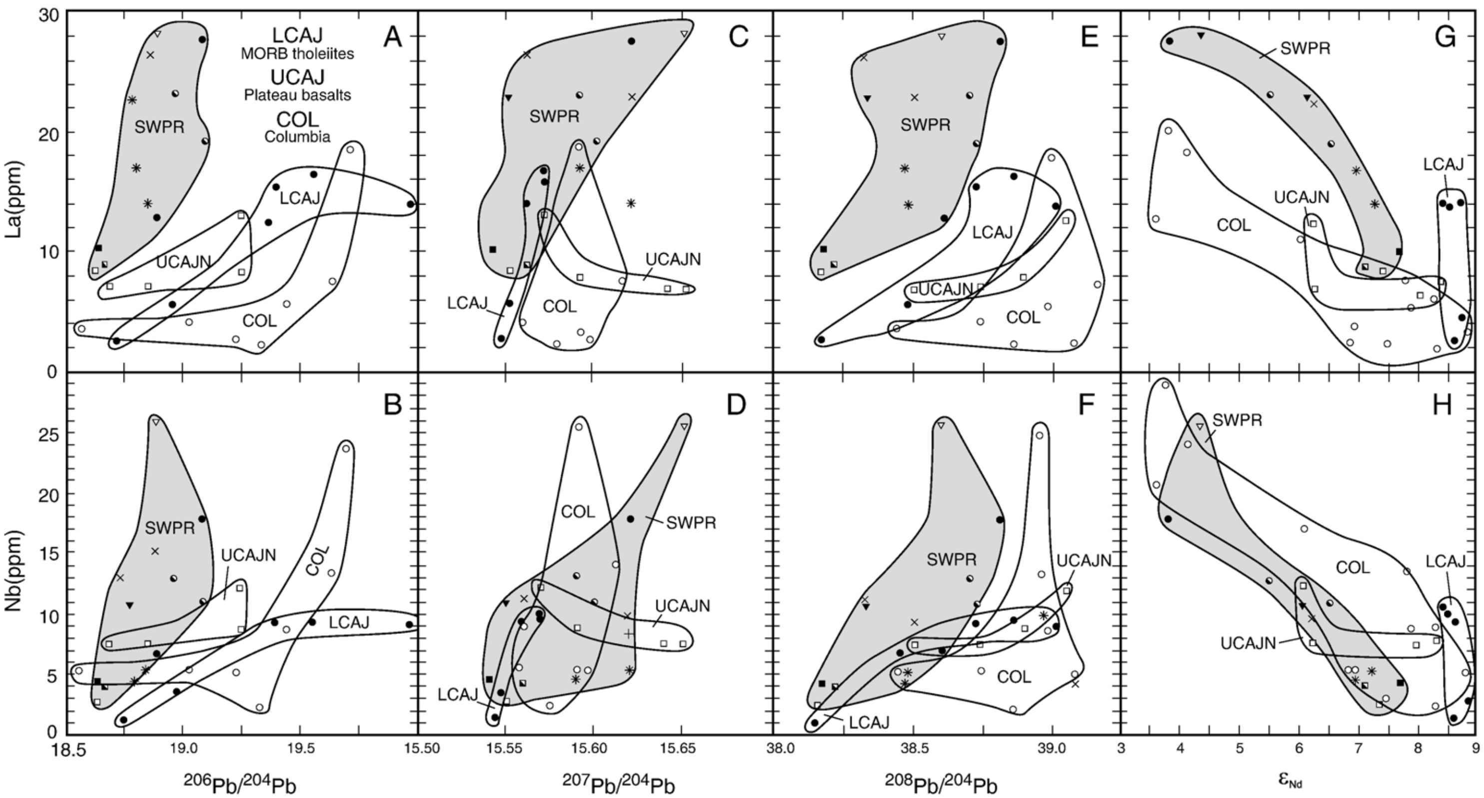

Fig. 9. Covariation of La and Nb with isotope ratios, including (A) $^{206}Pb/^{204}Pb$, (B) $^{207}Pb/^{204}Pb$, (C) $^{208}Pb/^{204}Pb$, and (D) ε_{Nd}, in southwest Puerto Rico lavas (shaded field) and basement rocks, including the Cajul Formation (UCAJ) and Columbian plateau basalts (Col). Unit codes are the same as in Fig. 6.

olivine stability field at the expense of orthopyroxene under water-present conditions at high pressures, produces melts with elevated SiO_2 and MgO concentrations, compared with melts generated in anhydrous and dehydrating systems, without significantly altering CaO/Al_2O_3 or FeO*/MgO. Second, geochemical (Defant and Drummond, 1990; Schiano et al., 1995) and experimental (Carroll and Wyllie, 1989; Sen and Dunn, 1994; Rapp and Watson, 1995; Rapp et al., 1999; Prouteau et al., 2001) evidence indicates that high-Mg andesite can also be generated through interaction of high-pressure slab melts with wedge peridotite in subduction zone settings.

High-Mg andesites of the second type are commonly associated with limited proportions of calc-alkaline lava thought to represent slab melts (adakites, Kay, 1980). Adakites are present in the forearcs of several Cenozoic subduction zones where they occur as vein glasses within olivine xenocrysts (Schiano et al., 1995), small-volume leucocratic veins (northern Kamchatka, Kapezhinskas et al., 1995), and lava flows (Aleutians, Kay, 1980; Southwest Japan; Morris, 1995; Philippines, Defant and Drummond, 1990; Sajona et al., 2000; Baja California, Mexico, Benoit et al., 2002). Because slab melts originate in a dehydrating slab and leave residual clinopyroxene and garnet (eclogite), adakites inherit several diagnostic geochemical features, including high SiO_2, Na_2O, and Al_2O_3, compared with typical island arc basalt. Adakites are most clearly distinguished by normalized trace element signatures with steep heavy rare earth element (HREE) slopes, elevated Sr/Y (<20) and La/Yb (>500), low Yb (<1 ppm), and negative Nb and Ti- and positive Zr-anomalies (Defant and Drummond, 1990; Prouteau et al., 2001).

High-Mg andesites from subduction zone settings normally have similar trace element compositions to associated adakite lavas, including elevated normalized REE slopes, negative Nb- and Ti- anomalies, positive Zr-anomalies, and relatively low absolute Yb concentrations (Yogodzinski et al., 1994, 1995; Tatsumi et al., 2002, 2003). The compositional parallels between adakites and high-Mg andesites within any given region indicate that slab melts interact with peridotite in the overlying wedge to form enriched source reservoirs that preserve key trace element features of the original adakite melts. In extreme cases, slab melts react with the mantle to produce high-Mg andesite through mantle assimilation, and fractional crystallization of orthopyroxene (western Aleutians, Yogodzinski et al., 1995; southwest Japan, Tatsumi, 2001; southern Chile, Stern and Kilian, 1996). This process was investigated experimentally by Carroll and Wyllie (1989), who demonstrated that mixtures of silicic melts and peridotite plot within the orthopyroxene field on high-pressure phase diagrams involving, for example, SiO_2, FeO*/MgO, and CaO. As a result the SiO_2 content and FeO*/MgO decreases and MgO increases in the reacting melts due to olivine dissolution and reactions such as olivine + SiO_2 → orthopyroxene. The extent of these reactions increases as the melts rise from the subducting slab into the central part of the mantle wedge, where higher temperatures prevail.

In all the above-mentioned Cenozoic island arc settings, high-Mg andesites and associated lavas are restricted to the forearc region, whereas more typical high-Fe island arc basalts, with comparatively elevated FeO*/MgO and Al_2O_3, are erupted in the arc-axis zone further from the trench. In comparison high-Mg andesites and hornblende-bearing lavas in Puerto Rico are localized within the southwestern-most corner of the island, whereas high-Fe basalts form an adjacent belt toward the northeast, an arrangement that implies northeast-dipping subduction of the Caribbean plate.

6.2. Southwest Puerto Rico

Experimental melts generated by high pressure (1.0 GPa) water-present partial fusion of depleted peridotite (sample KLB-1, Rapp et al., 1999) at temperatures between 975 and 1250 °C, closely resemble major element compositions of hornblende-bearing lavas from southwest Puerto Rico. For example, the rocks have high SiO_2 (up to 59%) and Al_2O_3 (16–21%), and low MgO (3–7%), whereas experimental melts (Hirose, 1997) contain from 53 to 61% SiO_2, 17 to 22% Al_2O_3, and 5 to 9% MgO (Fig. 5C, F). Early andesites from the Boqueròn Formation have the highest silica and most closely resemble water-present melts, whereas later lavas from the Sabana Grande and El Rayo Formations more closely resemble high-temperature melts. Despite the similarities, however, it is unlikely that any of these features can be attributed solely to melting under water-present conditions, since similar variations are produced both by fractional crystallization (fc in Fig. 5A, D) and introduction of slab melt (Fig. 5C, F).

An alternative mechanism of generating the Puerto Rican hornblende-bearing suite and associated high-Mg andesites is indicated by the trend of decreasing SiO_2 content from an average of 56% in the early lavas (Boquerón Formation) to 54% in the later units (El Rayo Formation). This trend produces a gradual displacement of individual hornblende-bearing units away from the slab melt field and toward anhydrous mantle melts on element–element plots, consistent with incorporation of decreasing proportions of slab melt. In comparison, high-Mg andesites are more enriched in SiO_2 (56–62%), reflecting a higher slab melt proportion. It is significant, however, that the high-Mg andesite field is off-set from the high-SiO_2 end of the hornblende basalt trend toward peridotite, consistent with mantle assimilation, as happens in Cenozoic arcs (Aleutians, Yogodzinski et al., 1994, 1995; southern Chile, Stern and Kilian, 1996; southwest Japan, Tatsumi et al., 2002).

Geophysical models (Peacock, 1993) indicate that slab melting is significant only in arc systems that have anomalously elevated geothermal gradients in the subducting lithosphere. Hence, Cenozoic high-Mg andesites are concentrated in geologic settings with relatively young oceanic crust (<25 Ma, Defant and Drummond, 1990), such as southwest Japan (Setouchi belt, Tatsumi, 2001; Tatsumi et al., 2002, 2003) and Okinawa (Shinjo, 1999), southwest Philippines (Sajona et al., 2000), Alexander Island, Antarctica (McCarron and Smellie, 1998), southern Chile (Stern and Kilian, 1996), Panama (Defant and Drummond, 1990), and Baja California (Benoit et al., 2002). Several of these arc segments subduct active ridge systems (southwest Japan, Philippines, and Antarctica) or other thermal anomalies (Baja). Additionally, a subset of Cenozoic arcs, including the western Aleutians (Yogodnzinski et al., 1994, 1995), the Philippines (Sajona et al., 2000) and southern Chile (Stern and Kilian, 1996), erupted in settings with oblique subduction, where long subduction tracks generate greater frictional heating of the upper slab (Peacock, 1993). In southwest Puerto Rico, the principal source of abnormal heat flow is inferred to have been emplacement of the Caribbean plume, but it seems likely that this event was supplemented by associated processes, such as introduction of heat by the ascent of high-temperature plume melts from depth and underplating by associated gabbroic sills.

6.3. Trace elements

Major element compositions of end-members involved in generation of high-Mg andesites in southwest Puerto Rico are not known with any degree of certainty. Hence, the petrogenesis of the rocks is more reliably assessed from the distribution of trace elements. Since the effects of variation in degree of melting and fractional crystallization are minimized by trace element ratios, emphasis in the following sections is placed on ratios of key elemental pairs. These include La/Sm and Sm/Yb, which represent chondrite-normalized slopes of LREE and HREE segments, respectively, and La/Nb and Zr/Sm, which reflect relative magnitudes of normalized Nb and Zr-anomalies. In addition Nb/Zr is utilized to characterize the degree of incompatible element source enrichment.

6.3.1. Geochemical parameters

The spinel lherzolite adopted for use in melting models consists of 57.5% olivine (ol), 27.0% orthopyroxene (opx), 12.5% clinopyroxene (cpx), and 3.0% spinel (McKenzie and O'Nions, 1991). Amphibole is not included because it is absent in high pressure experimental peridotite melts under hydrous conditions (Hirose, 1997). It is inferred that cpx disappears after 25% melting, opx after 40%, and Al-spinel after 80% (Pearce and Parkinson, 1993). It is also inferred that phases disappear from the source at constant rates, such that orthopyroxene is converted to olivine during early stages of fusion. REE partition coefficients (*D*-values) for fractional melting of spinel peridotite and fractional crystallization of basaltic melts are adopted from the set compiled by Pearce and Parkinson (1993) and modified by Bédard (1999). Values for equilibrium batch melting of the slab at high pressures, some of which are interpolated, are from the set developed in the western Aleutians (Yogodzinski et al., 1995; see also Münker et al., 2004). A large range of HFSE partition coefficients for residual ilmenite (ilm) and rutile have been published. For example, $D^{ilm}/_{Nb}$ values reported by Ewart and Griffin (1994) and Stimac and Hickmott (1994) range from 6.58 to 89.9 and 50.9 to 64.2, respectively. In comparison, a range in $D^{ilm}/_{Ta}$ from 64 to 85 was reported by Stimac and Hickmott, while an average of 106 was suggested by Nash and Crecraft (1985). Stimac and Hickmott reported an extended range of $D^{ilm}/_{Ti}$, from 150 to 200. An experimental value of $D^{rutile}/_{Ta}=44$ was measured in intermediate melts by Green and Pearson (1987). Values of 50 and 100 for Nb-Ta and Ti, respectively, representing the mid-range of published values, are adopted for slab melting models.

6.3.2. Melting models

Normalized incompatible element patterns like those of hornblende-bearing lavas and high-Mg andesites (Fig. 10B) can be produced by several multi-step processes, all involving introduction of a slab melt into an incompatible element-enriched mantle source, either prior to or during melting. It is significant that normalized REE patterns of high-Mg-basalts, which contain the smallest slab melt component, are subparallel to E-MORB. Moreover, the fields of Puerto Rican and Columbian plateau basalts are both closely associated with the E-MORB composition in trace element plots (Fig. 11a, b). Consequently, an inverted E-MORB composition (EMINV in Fig. 10) is selected to represent the starting wedge source composition in melting models. It was noted during modeling that small variations in starting composition have minimal effects on results, because elevated trace element concentrations in slab melts thoroughly dominate melting and mixing proportions. The degree of melting in the models is set at 20%, slightly above 15% estimates for Columbian plateau basalts (Kerr et al., 2002), to include a uniform correction for decompressive fractional crystallization during ascent of the melts, and to simplify the models, it

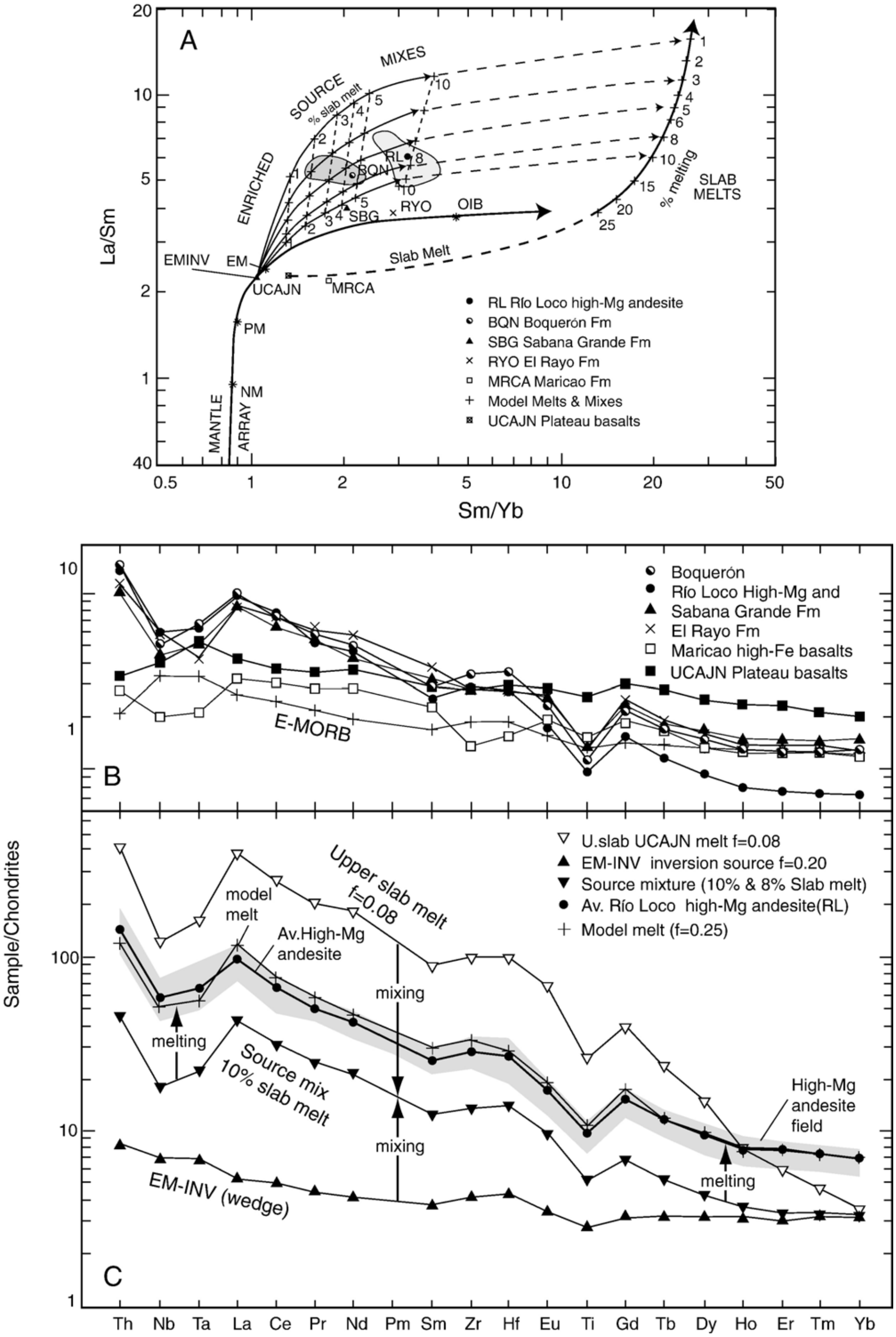

is inferred that the wedge was uniform in composition and that subducted pelagic chert did not contribute a significant sediment component.

The first step in the process is equilibrium modal melting of the slab, leaving an eclogitic residue (cpx/gt = 1; Yogodzinski et al., 1995). Green and Pearson (1987) and Ryerson and Watson (1987) demonstrated that experimental high-pressure hydrous basalt melts are saturated in rutile. Hence, small proportions of rutile (0.04%) are included in the residue. It was determined that normalized REE slopes generated from the northern facies of the Upper Cajul Formation (UCAJN) produces a range of patterns similar to observed high-Mg andesites and related lavas, whereas the more enriched southern facies produces patterns that are too steep. Hence, it is inferred that basalts similar to the northern facies dominated the melting process.

In step two, selected slab melts (f=0.01, 0.02, 0.03, 0.04, 0.06, 0.08, and 0.10 in Fig. 10A) are mixed with the inferred wedge source to produce a series of hybrid sources. On La/Sm vs. Sm/Yb plots, the resulting family of subparallel vectors form a grid from which both the degree of slab melting and the proportion of slab melt required to produce a given unit can be estimated. For example, the grid indicates that the Boqueròn source incorporated approximately 5% of a slab melt produced by 5% melting (f=0.05). In comparison, as much as 10% of a slightly higher degree slab melt (f=0.08) was incorporated by the high-Mg andesite source. It is noted that the lower normalized REE slopes characteristic of high-Fe basalt (Maricao Basalt) and late-stage hornblende-bearing lavas (Sabana Grande and El Rayo Formations) plot outside the field of predicted mixtures (Figs. 10A; 11C, D), consistent with the presence of an additional component, as discussed in Section 7.1.

The third step in the process includes fusion of the appropriate source mixture to produce model melts as indicated in Fig. 10A. Normalized results for 15% melting (f=0.25) reproduce elevated LREE slopes, shallow negative Nb- and Ti-anomalies, and slight positive Zr-anomalies characteristic of high-Mg andesite. It is unlikely that this simple process alone produced observed high-Mg andesites, however, since it generates melts with relatively elevated Al_2O_3, as in the hornblende-bearing suite. To obtain the characteristic low Al_2O_3 concentrations of high-Mg andesites an additional step, involving mantle-mass assimilation, is required. Acceptable results consistent with major element mixing models are obtained from slightly lower degree melts (f=0.15) than shown in (Fig. 10C) combined with mantle assimilation and fractional crystallization of various combinations of olivine and orthopyroxene. Identical patterns are produced by the reverse processes, involving mixing of a basaltic mantle melt with 20 to 30% slab melt followed by assimilation and fractional crystallization of olivine and orthopyroxene.

A profile of the hypothetical northeast-dipping subduction zone in southwest Puerto Rico consistent with the above melting parameters, modified from the generalized dynamic subduction model of Peacock (1993), is presented in Fig. 11. At point (a), hornblende basalts and andesites were generated in the forarc zone by melting of wedge peridotite that had incorporated up to 5% slab melt. At higher temperatures deeper in the subduction zone (b), up to 10% slab melt was introduced into the wedge. The resultant increase in buoyancy apparently destabilized the mantle and promoted upwelling accompanied by mantle-mass assimilation and fractional crystallization of orthopyroxene ultimately producing high-Mg andesites. Still deeper in the subduction zone (c), normal aqueous flux-related melting processes produced high-Fe basalts in the arc-axis zone.

7. Tectonic implications

7.1. Supra-subduction zone component

Establishment of a northeast-dipping subduction zone along the south flank of the northeast Antilles platform during the Santonian, and its persistence through at least Maastrichtian times (85–65 Ma), are inconsistent with tectonic models involving a shift from north- to south-dipping subduction in the Antilles during the Campanian. Instead, the arrangement implies that older Albian

Fig. 10. A) Covariation of La/Sm and Sm/Yb. Slab melt vectors (f=0.01, 0.02, 0.03, 0.04, 0.05, 0.06, 0.08, 0.10, 0.20, 0.25) produced by fusion of the average plateau basalt (UCAJN) are compared with the mantle array (Sun and McDonough, 1989) and tracks (1, 2, 3, 4, 5, 10% slab melt) for mixtures between the inferred wedge source and various slab melt fractions (f=0.01, 0.02, 0.03, 0.04, 0.05, 0.10). The high-Mg andesite composition and the field of the Río Loco Formation are located near the 10% slab melt contour (f=0.08), consistent with models presented in Fig. 10C, whereas the average Boquerón lava plots between the 2 and 5% slab melt vectors (f=0.05). (B) Chondrite normalized incompatible element–element patterns of average lava units in southwest Puerto Rico compared with E-MORB (Sun and McDonough, 1989). (C) N-MORB-normalized petrogenetic models for generation of high-Mg andesites (Río Loco Formation), involving the following: 1) mixing between an E-MORB inversion source (f=0.2) and 10% slab melt generated by high-pressure fusion (f=0.08) of basalts from the Upper Cajul Formation to form an enriched source; 2) fusion (f=0.25) of the enriched source to form a model liquid with normalized incompatible element patterns closely resembling observed high-Mg andesites.

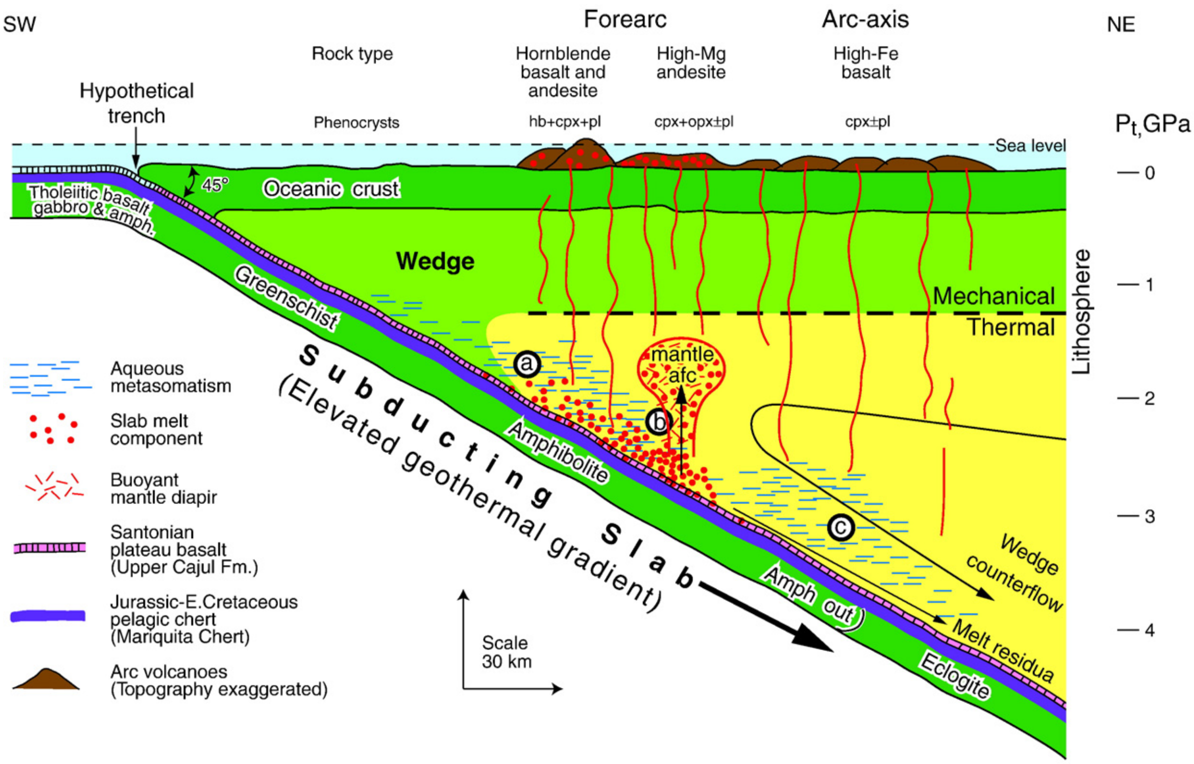

Fig. 11. Dynamic supra-subduction zone model (mantle parameters modified from Peacock, 1993; Pearce and Parkinson, 1993). Subduction involves hot lithosphere, heated by simultaneous emplacement of the Caribbean Cretaceous Mantle Plume in the adjacent Caribbean Basin. Subducted crustal strata include, from the base upward, tholeiitic basalts and intrusive equivalents forming the bulk of the lower slab, refractory pelagic chert Mariquita Chert (SiO_2=95–100%), and within-plate basalt representing a local facies of the Caribbean basalt plateau, forming the upper slab. Slab melts, derived by low-degree fusion (f=0.08) of the upper slab, reacted with the overlying mantle wedge, forming enriched source reservoirs. A trenchward belt (point a) of hornblende-bearing forearc lavas (Boquerón, Sabana Grande, and El Rayo Formations) incorporated up to 5% slab melt, whereas high-Mg andesites from the central volcanic belt (Río Loco Formation) incorporated as much as 10% slab melt (point b). High-Mg, low-Al_2O_3 andesite was generated by a combination of gravitational mobilization of the more buoyant enriched source, accompanied by mantle-mass assimilation and orthopyroxene fractional crystallization (AFC ≈ 1). At greater depths aqueous fluid-related fusion generated high-Fe basalt in the arc axial zone (point c).

to Cenomanian arc strata in eastern Puerto Rico, dating from >110 Ma (Fig. 2), were produced by an opposing southwest-dipping subduction zone that had already been operative for at least 20 million years when the Caribbean basalt plateau was erupted (92–88 Ma, Révillon et al., 2000). Hence, the emplacement of the Caribbean mantle plume and subsequent arc volcanism (from ~85 Ma, Schellekens, 1991) both occurred within the broad back-arc or supra-subduction zone region of the older southwest-dipping arc system where permeating aqueous fluids and melts from the underlying Benioff zone are expected to overprint the upper mantle with an arc signature (Rodkin and Rodkinvo, 1996), which is most prominently characterized by negative normalized HFSE-anomalies (Taylor and Martinez, 2003). The absence of a recognizable supra-subduction zone component in Caribbean plateau basalts outside of Puerto Rico (Kerr et al., 2002), has favored tectonic models involving persistent northeast-dipping subduction like those of Lapierre et al. (1997, 1999), Révillon et al. (2000), and Kerr and Tarney (2005).

Detection of a supra-subduction zone component is inherently difficult in incompatible element-enriched rocks, because elevated trace element and radiogenic isotope abundances in the protolith dominate mixing proportions. The problem is simplified considerably in southwest Puerto Rico, because the subducted Pacific pelagic chert was highly refractory and infertile with respect to incompatible elements and is unlikely to have contributed a significant subduction-related component. Pelagic sediments in the Cretaceous Atlantic basin, in contrast, were dominated by high REE and low HFSE biogenic and calcareous claystone (Donnelly, 1978) with unusually high La/Nb and low Zr/Sm (Jolly et al., 2001, 2006). Accordingly, trace element ratios potentially provide convenient markers of pelagic sediments originating in the Atlantic basin. For instance, La/Nb, which reflects the relative magnitude of negative normalized Nb-anomalies, is significantly higher in plateau basalts from the Upper Cajul Formation (UCAJN in Fig. 12) than in Columbian counterparts. Moreover, the Puerto Rican field is off-set in La/Nb-Nb/Zr plots (Fig. 12A) away from the mantle array and other mantle basalts toward Atlantic Cretaceous pelagic sediment (AKPS), consistent with the presence of a small supra-subduction zone component of Atlantic origin. Similarly, Columbian plateau basalts concentrate above the mantle trend on La/Sm-Zr/Sm plots, whereas the fields of Puerto Rican and central Caribbean plateau basalts are significantly off-set below the mantle trend toward Atlantic sediment (Fig. 12B). Relative to a simple mixing line between an inferred plume source (Zr/Sm = 28) and biogenic Atlantic sediment (sample DSDP 417/19/1 in Jolly et al., 2006), Zr/Sm in the Puerto Rican suite is consistent with a sediment content of approximately 0.5% (Fig. 12C).

On La/Sm-Zr/Sm plots (Fig. 12C) arc lavas from southwest Puerto Rico form an elongate envelope with Zr/Sm values ranging from >28 in the forearc to <15 in the arc-axis zone. The distribution of ε_{Nd} with respect to Zr/Sm produces similar patterns (Fig. 12D). The large range of Zr/Sm values is inconsistent with fractional crystallization of any likely combination of phenocrysts (see vectors in Fig. 12C). In addition, the low SiO_2 content of the high-Fe basalts is inconsistent with significant contamination by low-degree crustal melts. Instead the extended Puerto Rican field resembles a mixing trend between a Boquerón-like source containing 5% slab melt and a mantle wedge source containing a small supra-subduction zone component. The

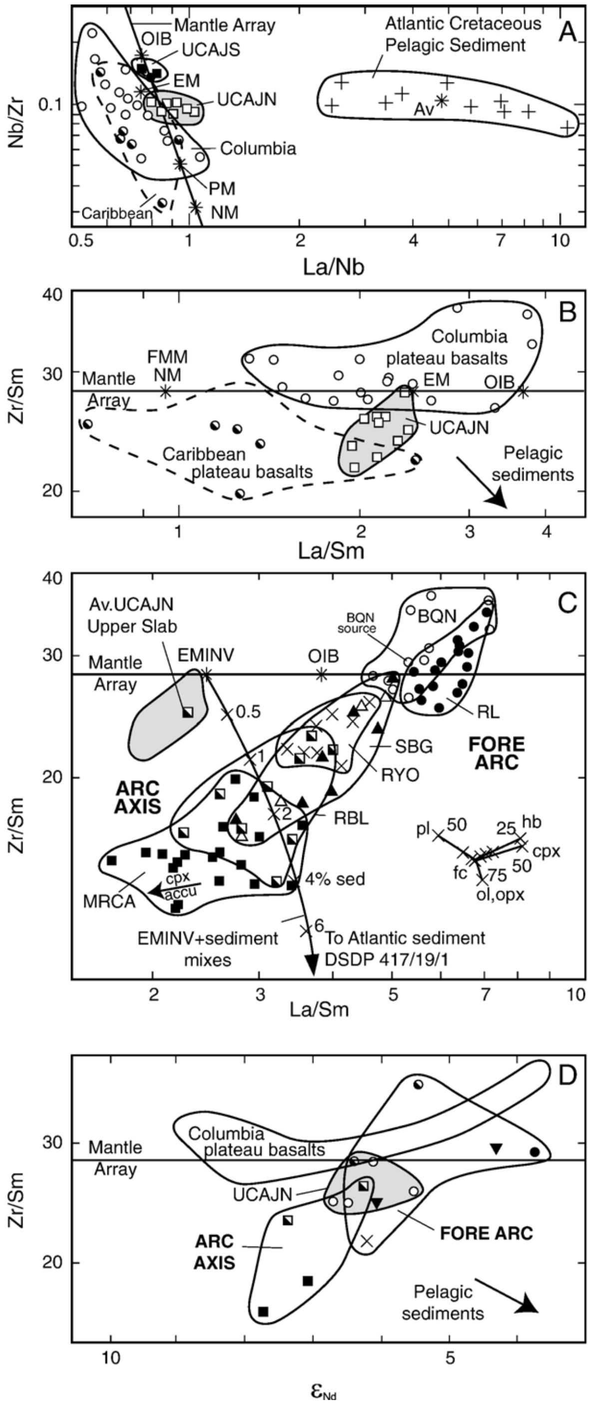

Fig. 12. (A) Covariation of La/Nb and Nb/Zr in the Caribbean Cretaceous basalt plateau. Samples are from the Columbian basalt plateau (Kerr et al., 2002), the central Caribbean basalt plateau (DSDP samples, Jolly and Lidiak, 2006), and the Upper Cajul Formation in southwest Puerto Rico (UCAJ, northern and southern facies, N and S, respectively). Also included for reference is the field of Atlantic Cretaceous pelagic sediments (AKPS) from Jolly et al. (2006). (B) Geochemical data from the Caribbean basalt plateau; units are identified as in (A) above. Jurassic MORB tholeiites from the pre-arc basement in southwest Puerto Rico (Jolly and Lidiak, 2006) are included for reference. (C) Covariation of La/Sm and Zr/Sm in lavas from southwest Puerto Rico. Units include the Boquerón (BQN), Río Loco (RL, high-Mg andesite), Sabana Grande (SBG), El Rayo (RYO), Maricao (MRCA), and Río Blanco (RBL) Formations. Fractionation vectors and mantle components are as described in Fig. 5. Also included is a two-component mixing line between an E-MORB-type source and calcareous Atlantic Cretaceous pelagic sediment (sample DSDP 417/19/1, Jolly et al., 2006). The intersection of the Puerto Rican trend with the source-plus-sediment mixing line is consistent with from 1 to 2% sediment. Note that the flattening of the low Zr/Sm end of the high-Fe basalt field reflects the presence of large proportions (up to 40%) of accumlitic augite. (D) Covariation of Zr/Sm and ε_{Nd} in SWPR lavas compared with Puerto Rican and Columbian plateau basalts (Kerr et al., 2002); symbols the same as in (B).

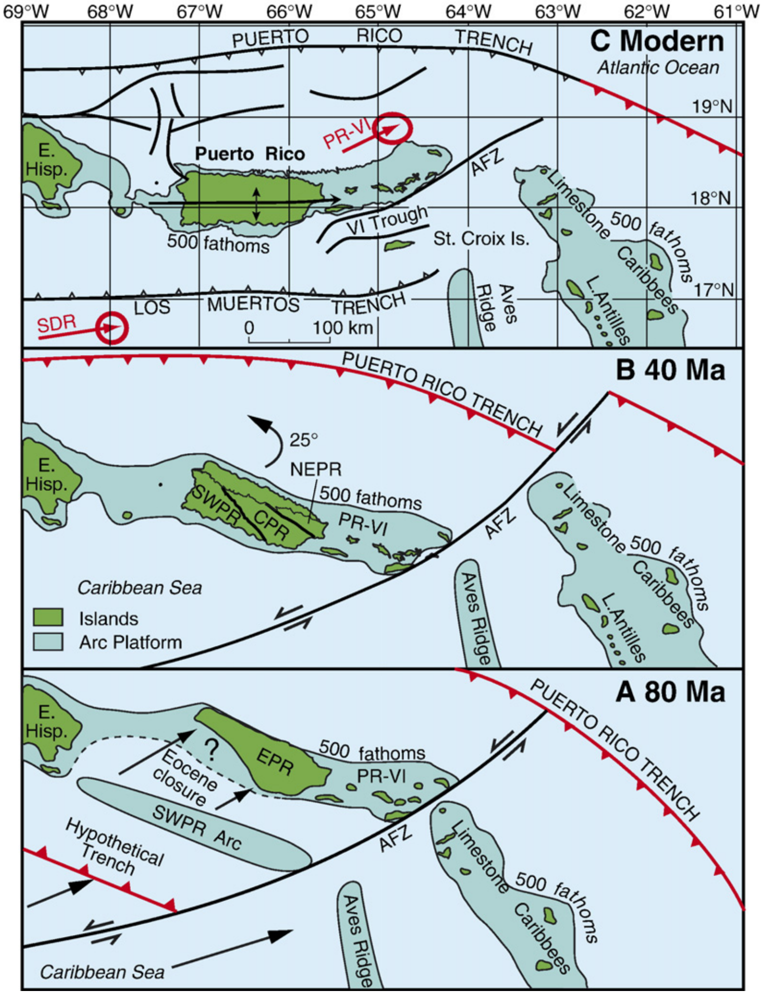

Fig. 13. (A) Inception of the northeast-dipping southwest Puerto Rico island arc system (85 Ma), illustrating the location of the hypothetical trench, original configuration of the northeast Antilles platform and submarine Aves Ridge, and Eocene closure of the intra-arc basin. (B) Northeastern Antilles arc platform (40 Ma), preceding 25° anticlockwise Miocene rotation (modified from Larue and Ryan, 1998), indicating a 250 km left-lateral off-set of the platform along the ancestral Anegada Fracture Zone (AFZ). (C) Modern arrangement of the Puerto Rico–Virgin Island (PR-VI) and Lesser Antilles segments of the Antilles arc platform (modified from Larue and Ryan, 1998) as defined by the 500 fathom bathometric contour; vectors from Jansma et al. (2000). Geological features are identified in Fig. 1.

intersection of the Puerto Rican trend with the source-plus-Atlantic sediment mixing line is consistent with the presence of approximately 1.5% sediment. This supra-subduction zone component is strongly masked in units with >5% slab melt, such as the Boquerón and Río Loco Formations. However, the narrow field of the Puerto Rican suite indicates that the component was distributed relatively homogeneously throughout the mantle wedge.

7.2. Tectonic setting

To accommodate a supra-subduction zone component of Atlantic origin in southwest Puerto Rico, potential tectonic models must include persistent southwest-dipping subduction along the northern flank of the older northeast Antilles arc platform during early stages of arc development. Moreover, the geochemical continuity of volcanism in eastern Puerto Rico during the Cenomanian to Campanian interval (Jolly et al., 2006) indicates that the two opposing arcs systems were operating simultaneously during the latter part of that period. One of the simplest tectonic models (Fig. 13) consistent with these constraints involves a lag in eastward motion of the northeast Antilles compared with the adjacent Limestone Caribees segment of the arc system, beginning in Santonian time. Possible mechanisms include an increase in frictional resistance along the northern sector of the arc due to increased obliquity of subduction or to interaction of the Greater Antilles sector of the arc with Central America as the platform swept past the southern fringes of the North American Plate. Eastward convergence in the central Caribbean may also have been supplemented by early spreading along the Caiman trough (Pindell et al., 2005).

As a result of these or other factors, a new northeasterly-dipping subduction zone was established on the southern flank of the Greater Antilles arc platform to absorb excess convergence (Fig. 13C). Meanwhile, the Limestone Caribees and central Caribbean region, isolated from the Greater Antilles by an ancestor of the modern Anegada Fault Zone (Pindell et al., 2005), proceeded to drift eastward, ultimately producing a 250 km left-lateral off-set of the arc platform (Fig. 13B). The submarine Aves Ridge, located near the southern terminus of the southwest Puerto Rico arc in this reconstruction, possibly represents an extension of northeast-dipping subduction into the Caribbean Basin, as suggested by Donnelly (1989) and Schellekens (1998). High-Mg andesites are not recognized in southern Hispaniola, situated across Mona Passage west of Puerto Rico (Figs. 1, 13A), possibly because correlative Cretaceous strata were obscured in Miocene time (Mauffret and Jany, 1990; Mann et al., 1991) when the Beata Ridge overrode southern Hispaniola. However, Lapierre et al. (1997, 1999) suggested that a thicker, more buoyant sequence of the Caribbean basalt plateau, together with its underlying basement complex, was accreted in southern Hispaniola during an earlier Campanian episode of north-directed overthrusting (see also Kerr and Tarney, 2005; for a contrary view see Lewis et al. 1999). If so, this obduction event was probably coincident with subduction of the much thinner sequence of plateau basalts in southwest Puerto Rico.

8. Conclusions

Island arc strata in southwest Puerto Rico, dating between 85 and 65 Ma, are subdivided into three southeast-trending volcanic belts with distinctive rock types. These include, from southwest to northeast, hornblende-bearing basalts and andesites, two-pyroxene high-Mg andesites, and high-Fe basalts. By analogy with tectonic settings of Cenozoic island arcs, this distribution implies that the polarity of subduction in southwest Puerto Rico was northeast-dipping. The upper subducting slab in such a setting consisted of highly refractory Jurassic and Cretaceous pelagic chert (Mariquita Chert) and an overlying succession of plateau basalts (Upper Cajul Formation), representing a local facies of the Caribbean basalt plateau (93–88 Ma). This arrangement is consistent with incompatible trace element melting models for high-Mg andesites and associated hornblende-bearing lavas that require introduction of a slab melt component generated by high-pressure melting of subducted plateau basalts. The models indicate that hornblende-bearing lavas incorporated up to 5% of a 5% slab melt ($f=0.05$). In comparison, parental melts of high-Mg andesite, generated at deeper levels, incorporated up to 10% slab melt ($f=0.08$). Elevated buoyancy of the more highly enriched high-Mg andesite source gravitationally destabilized the mantle wedge, leading to extensive mantle-mass assimilation and the characteristic high-MgO and low Al_2O_3 concentrations. High-Fe basalts were generated at still deeper levels of the subduction zone, where slab melt was replaced as the principal fluxing agent by aqueous fluids emanating from the dehydrating slab. Geophysical models (Peacock, 1993) indicate that slab melting requires elevated heat flow in the subducting lithosphere. In most Cenozoic arc settings, the abnormal heat flow required to trigger slab melting is traced predominantly to subduction of young, hot oceanic plates or active spreading ridges. In contrast, the apparent source of elevated heat flow in the ancient Jurassic Caribbean Plate was emplacement of the Caribbean mantle plume (93–75 Ma, Hauff et al., 1999), supplemented by ascent of plume basalts from depth and gabbroic underplating, immediately preceding arc volcanism (from 85 Ma). The presence of a high Zr/Sm supra-subduction zone component of Atlantic origin in Caribbean plateau basalts and arc lavas from southwest Puerto Rico is consistent with development of the arc within the broad back-arc region of an older, south-dipping arc system in eastern Puerto Rico.

Acknowledgements

The authors are grateful to colleagues in the Caribbean for discussions of high-Mg andesites and the Caribbean plateau, and to two anonymous reviewers for helpful and thorough reviews of the manuscript. Financial support for this project is provided through Discovery Grants by the National Science and Engineering Council of Canada (NSERC). Graphics were prepared by M. Lozon of the Department of Earth Sciences, Brock University.

Appendix A. Supplementary data

Supplementary data associated with this article can be found, in the online version, at doi:10.1016/j.lithos.2007.01.011.

References

Arculus, R.J., 1994. Aspects of magma genesis in arcs. Lithos 33, 189–208.

Arculus, R.J., 2003. Use and abuse of the terms calcalkaline and calcalkalic. Journal of Petrology 44, 929–935.

Bawiec, 2001. Geology, Geochemistry, Geophysics, Mineral Occurrences, and Mineral Resource Assessment for the Commonwealth of Puerto Rico (ed.). U. S. Geological. Survey, Open File Report CD-ROM, 98–38.

Bédard, J.H., 1999. Petrogenesis of boninites from the Betts Cove Ophiolite, Nfld, Canada: identification of subducted source components. Journal of Petrology 40, 1853–1889.

Benoit, M., Aguillón-Robles, A., Calmus, T., Maury, R., Bellon, H., Cotten, J., Bourgois, J., Michaud, F., 2002. Geochemical diversity of Late Miocene volcanism in Southern Baja California, Mexico: implication of mantle and crustal sources during the opening of an asthenospheric window. Journal of Geology 110, 627–648.

Boynton, C.H., Westbrook, G.K., Bott, M.H.P., 1979. A seismic refraction investigation of crustal structure beneath the Lesser Antilles island arc. Geophysical Journal of the Royal Astronomical Society 58, 371–393.

Burke, K., 1988. Tectonic evolution of the Caribbean. Annual Reviews of Earth and Planetary Sciences 16, 201–230.

Carroll, M.R., Wyllie, P.J., 1989. Experimental phase relations in the system tonalite-peridotite-H_2O at 15 kb: Implications for assimilation and differentiation processes near the crust–mantle boundary. Journal of Petrology 30, 1351–1382.

Cox, D.P., Marvin, R.F., McGonigle, J.W., McIntyre, D.H., Rogers, C.I., 1977. Potassium-argon geochemistry of some metamorphic, igneous, and hydrothermal events in Puerto Rico and the Virgin Islands. U. S. Geological Survey Journal of Research 5 (56 pp.).

Defant, M.J., Drummond, M., 1990. Derivation of some modern arc magmas by melting of young subducted lithosphere. Nature 347, 662–665.

Dolan, J., Mann, P., de Zoeten, R., Heubek, C., Shiroma, J., 1991. Sedimentologic, stratigraphic, and tectonic synthesis of Eocene–Miocene sedimentary basins, Hispaniola and Puerto Rico. Geological Society of America Special Paper 262, 217–263.

Donnelly, T.W., 1978. Chemistry of sediments of the western Atlantic: site 417 compared with sites 9, 105, 386, 387. Initial Reports of the Deep Sea Drilling Project 51B53, 1515–1523.

Donnelly, T.W., 1989. Geologic history of the Caribbean and Central America. In: Bally, A.W., Palmer, A.R. (Eds.), Geology of North America—An Overview. Geological Society of America Special Paper A, pp. 299–321.

Donnelly, T.W., Thompson, G., Salisbury, H., 1978. The chemistry of altered basalts at site 417, leg 51. Initial Reports of the Deep Sea Drilling Project 51–53, 1319–1330.

Dosso, L., Bougault, H., Joron, J.-L., 1993. Geochemical morphology of the North mid-Atlantic ridge, 10–24°: trace element-isotope complementarity. Earth and Planetary Science Letters 120, 443–462.

Draper, D.S., Johnston, A.D., 1992. Anhydrous PT phase relations of an Aleutian high-MgO basalt: an investigation of the role of olivine-liquid reaction in the generation of arc high-alumina basalts. Contributions to Mineralogy and Petrology 112, 501–519.

Draper, G., Guitierrez, G., Lewis, J.F., 1996. Thrust emplacement of the Hispaniola peridotite belt: orogenic expression of the mid-Cretaceous Caribbean arc polarity reversal. Geology 24, 143–1146.

Ellam, R.M., Hawkesworth, C.J., 1988. Elemental and isotope variations in subduction related basalts: evidence of a three-component model. Contributions to Mineralogy and Petrology 98, 72–80.

Erikson, J.P., Pindell, J.L., Larue, D.K., 1990. Mid-Eocene-Early Oligocene sinistral transcurrent faulting in Puerto Rico associated with formation of the northern Caribbean plate boundary zone. Journal of Geology 98, 365–384.

Ewart, A., Griffin, W.L., 1994. Application of proton-microprobe data to trace-element partitioning in volcanic rocks. Chemical Geology 117, 251–284.

Frost, C.D., Schellekens, J.H., 1991. Rb–Sr and Sm–Nd isotopic characterization of Eocene volcanic rocks from Puerto Rico. Geophysical Research Letters 18, 545–548.

Frost, C.D., Schellekens, J.H., 1998. Nd, Sr, and Pb isotope characterization of Cretaceous and Paleogene volcanic and plutonic island arc rocks from Puerto Rico. Geological Society of America Special Paper 322, 123–132.

Gill, J.B., 1981. Orogenic Andesites and Plate Tectonics. Berlin, Springer.

Gradstein, F.M., Ogg, J.G., Smith, A.G., et al., 2004. A Geologic Time Scale. Cambridge University Press, Cambridge.

Green, D.H., Pearson, 1987. An experimental study of Nb and Ta partitioning between Ti-rich minerals and silicate liquids at high pressure and temperature. Contributions to Mineralogy and Petrology 91, 24–36.

Hart, S.R., 1984. A large-scale isotope anomaly in the southern hemisphere mantle. Nature 309, 753–757.

Hauff, F., Hoernle, K., Tilton, G., Graham, D.W., Kerr, A.C., 2000. Large volume recycling of oceanic lithosphere over short time scales: geochemical constraints from the Caribbean Large Igneous Province. Earth and Planetary Science Letters 174, 247–263.

Hirose, K., 1997. Melting experiments on lherzolite KLB-1 under hydrous conditions and generation of high-magnesian andesitic melts. Geology 25, 42–44.

Iturralde-Vinent, M.A., McPhee, R.D.E., 1999. Paleogeography of the Caribbean region: Implications for Cenozoic biostratigraphy. American Museum of Natural History Bulletin 238, 1–95.

Jansma, P., Mattioli, G., Lopez, A., DeMets, C., Dixon, T.H., Mann, P., Calais, E., 2000. Neotectonics of Puerto Rico and the Virgin Islands, northeastern Caribbean, from GPS geodesy. Tectonics 19, 1021–1037.

Jolly, W.T., Lidiak, E.G., 2006. Role of crustal melting in petrogenesis of the Cretaceous Water Island Formation (Virgin Islands, northeast Antilles Arc). Geologica Acta 4, 7–34.

Jolly, W.T., Lidiak, E.G., Schelleckens, H.S., Santos, S., 1998. Volcanism, tectonics, and stratigraphic correlations in Puerto Rico. Geological Society of America Special Paper 322, 1–34.

Jolly, W.T., Lidiak, E.G., Dickin, A.P., Wu, T.-W., 2001. Secular geochemistry of central Puerto Rican island arc lavas: constraints on Mesozoic tectonism in the Greater Antilles. Journal of Petrology 42, 2197–2214.

Jolly, W.T., Lidiak, E.G., Dickin, A.P., 2006. Cretaceous to mid-Eocene pelagic sediment budget in Puerto Rico and the Virgin Islands (northeastern Antilles Island Arc). Geologica Acta 4, 35–62.

Kapezhinskas, P.K., Defant, M.J., Drummond, M.S., 1995. Na metasomatism in the island-arc mantle by slab melt-peridotite interaction: evidence from mantle xenoliths in the North Kamchatka Arc. Journal of Petrology 36, 1505–1527.

Kay, R.W., 1980. Volcanic arc magmas: implications of a melting-mixing model for element recycling in the crust-upper mantle system. Journal of Geology 88, 497–522.

Kerr, A.C., Tarney, J., 2005. Tectonic evolution of Caribbean and northwestern South America: the case for accretion of two Late Cetaceous oceanic plateaus. Geology 33, 269–272.

Kerr, A.C., Iturralde-Vinent, M.A., Saunders, A.D., Babbs, T.L., Tarney, J., 1999. A new plate tectonic model of the Caribbean: implications from a geochemical reconnaissance of Cuban Mesozoic volcanic rocks. Geological Society of America Bulletin 111, 1581–1599.

Kerr, A.C., Tarney, J., Kempton, P.D., Spaden, S., Nivia, A., Marriner, G.F., Duncan, R.A., 2002. Pervasive mantle plume head heterogeniety: Evidence from the late Cretaceous Caribbean–Columbian oceanic plateau. Journal of Geophysical Research 107 (B7), ECV2–1-13. doi:10.1029/2001JB000790.

Kesler, S.E., Campbell, I.H., 2005. Age of the Los Ranchos Formation, Dominican Republic, Central Greater Antilles. Geological Society of America Bulletin 61, 668–682.

Krushensky, R.D., Monroe, W.H., 1978. Geologic map of the Yauco and Punta Verraco quadrangles, Puerto Rico. United States Geological Survey Miscellaneous Geological Investigations Map I-1147.

Kushiro, I., 1974. Melting of hydrous upper mantle and possible generation of andesitic magmas. Earth and Planetary Science Letters 22, 294–299.

La Maitre, R.W., 1989. A Classification of Igneous Rocks and Glossary of Terms. Blackwell, Oxford. 193 pp.

Lapierre, H., Dupuis, V., Lepinay, B.M., Tardy, M., Ruiz, J., Maury, R.C., Hernandez, J., Loubert, M., 1997. Is the Lower Duarte Complex (Hispañiola) a remnant of the Caribbean plume generated oceanic plateau? Journal of Geology 105, 111–120.

Lapierre, H., Dupuis, V., Lepinay, B.M., Bosch, D., Moni, P., Tardy, M., Maury, R.C., 1999. Late Jurassic oceanic crust and Upper Cretaceous Caribbean Plateau picritic basalts exposed in the Duarte igneous complex, Hispañiola. Journal of Geology 107, 193–207.

Larue, D.K., Ryan, H., 1998. Seismic reflection profiles of Puerto Rican Trench: shortening between the North American and Caribbean plates. Geological Society of America Special Paper 332, 193–210.

Lewis, J.F., Hames, W.E., Draper, G., 1999. Late Jurassic oceanic crust and Upper Cretaceous Caribban plateau picritic basalts exposed in the Duarte igneous complex, Hispaniola: a discussion. Journal of Geology 107, 505–508.

Lewis, J.F., Escuder, J., Virtuete, P.P., Hernaiz Huerta, G., Gutierrez, G., Draper, G., Prez-Estan, A., 2002. Subdivisión geoquímica del Arco Isla Circum-Caribe, Cordillera Central Dominicana: Implicaciones para la formación, acreción, y crecimiento cortal en un ambiente intraoceanico. Acta Geologica Hispanica 37, 81–122.

Lidiak, E.G., Jolly, W.T., 1996. Circum-Caribbean granitoids: characteristics and origin. International Geological Reviews 38, 1098–1133.

McCarron, J.J., Smellie, J.L., 1998. Tectonic implications of fore-arc magmatism and generation of high-magnesian andesites; Alexander Island, Antarctica. Journal of the Geological Society of London 155, 269–280.

Mann, P., Draper, G., Lewis, J.F., 1991. An overview of the geologic and tectonic development of Hispaniola. Geological Society of America Special Paper 262, 1–28.

Mattson, P.H., 1960. Geology of the Mayagüez area, Puerto Rico. Geological Society of America Bulletin 71, 319–362.

Mattson, P.H., 1979. Subduction, buoyant braking, flipping, and strike-slip faulting in the northern Caribbean. Journal of Geology 87, 293–304.

Mauffret, A., Jany, I., 1990. Collision et tectonic d'expulsion le long de la frontiere Nord-Caraibe. Oceaniligica Acta 1, 97–116.

McIntyre, D.H., 1974. Concepción and Palma Escrita Formations, western Puerto Rico. United States Geological Survey Bulletin 1394-D, D1–D9.

McKenzie, D., O'Nions, R.K., 1991. Partial melt distributions from inversion of rare earth element concentrations. Journal of Petrology 32, 1021–1091.

Miyashiro, A., 1974. Volcanic rock series in island arcs and continental margins. American Journal of Science 274, 321–355.

Montgomery, H., Pessagno, E.A., Lewis, J.F., Schellekens, J.H., 1994. Paleogeography of Jurassic fragments in the Caribbean. Tectonics 13, 725–732.

Morris, P.A., 1995. Slab melting as an explanation of Quaternary volcanism and aseismicity in southwest Japan. Geology 23, 395–398.

Münker, C., Wörner, G., Yogodzinski, G., Churikova, T., 2004. Behaviour of high field strength elements in subduction zones: constraints from Kamchatka–Aleutian arc lavas. Earth and Planetary Science Letters 224, 275–293.

Mysen, B.O., Boettcher, A.L., 1975. Melting of a hydrous mantle. Journal of Petrology 16, 549–593.

Nash, W.P., Crecraft, H.R., 1985. Partition coefficients for trace elements in silicic magmas. Geochimica et Cosmochimica Acta 49, 309–322.

Peacock, S., 1993. Large-scale hydration of the lithosphere above subducting slabs. Chemical Geology 108, 49–59.

Pearce, J.A., Parkinson, I.J., 1993. Trace element models for mantle melting: application to volcanic arc petrogenesis. Geological Society of London Special Paper 76, 373–403.

Peccerillo, A., Taylor, S.R., 1976. Geochemistry of Eocene volcanic rocks from the Kastamonu area, northern Turkey. Contributions to Mineralogy and Petrology 58, 63–81.

Pindell, J.L., Barrett, S.F., 1990. Geological evolution of the Caribbean region: a plate tectonic perspective. Geological Society of America Special Paper H 405–432.

Pindell, J.L., Kennan, L., Maresch, W.V., Stanek, K.P., Draper, G., Higgs, R., 2005. Plate-kinematics and crustal dynamics of circum-Caribbean arc-continent interactions. Geological Society of America Special Paper 394, 7–52.

Pindell, J.L., Kennan, L., Stanek, K.P., Maresch, W.V., Draper, G.G., 2006. Foundations of Gulf of Mexico and Caribbean Evolution: eight controversies resolved. Acta Geologica 4, 303–341.

Prouteau, G., Scallet, B., Pichavant, M., Maury, R., 2001. Evidence for mantle metasomatism by hydrous silicic melts derived from subducted oceanic crust. Nature 410, 197–200.

Rapp, R.P., Watson, E.B., 1995. The amphibole-out phase boundary in partially melted metabasalt at 8–32 kbar: implications for continental growth and crust–mantle recycling. Journal of Petrology 36, 891–931.

Rapp, R.P., Shimizu, N., Norman, M.D., Applegate, G.S., 1999. Reaction between slab-derived melts and peridotite in the mantle wedge: experimental constraints at 3.8 GPa. Chemical Geology 160, 335–356.

Révillon, S., Hallot, E., Arndt, N.T., Chauvel, C., Duncan, R.A., 2000. A complex history for the Caribbean Plateau: Petrology, Geochemistry, and Geomorphology of the Beata ridge, South Hispaniola. Journal of Geology 108, 641–666.

Rodkin, M.V., Rodkinvo, A.G., 1996. Origin and structure of back-arc basins: new data and model discussion. Physics of the Earth and Planetary Interiors 93, 123–131.

Rollinson, H., 1998. Using geochemical data: evaluation, presentation, interpretation. Longman, London. 260 pp.

Ryerson, F.J., Watson, E.B., 1987. Rutile saturtion in magmas: implications for Ti-Nb-Ta depletion in island-arc basalts. Earth and Planetary Science Letters 86, 225–239.

Sajona, F.G., Maury, R., Proteau, G., Cotten, J., Schiano, P., Bellon, H., Fontaine, L., 2000. Slab melt as metasomatic agent in island arc magma mantle sources: Negros and Batan (Philippines). The Island Arc 9, 472–486.

Santos, H., 1999. Stratigraphy and depositional history of the Upper Cretaceous strata in the Cabo Rojo-San German structural block, southwestern Puerto Rico. Ph.D Dissertation, University of Colorado, Boulder CO.

Schellekens, J.H., 1991. Late Jurassic to Eocene geochemical evolution of volcanic rocks of Puerto Rico. Geophysical Research Letters 18, 523–556.

Schellekens, J.H., 1993. Geochemical evolution of volcanic rocks in Puerto Rico. Ph.D. Dissertation, Syracuse University, Syracuse NY.

Schellekens, J.H., 1998. Geochemical evolution and tectonic history of Puerto Rico. Geological Society of America Special Paper 322, 35–66.

Schellekens, J.H., Montgomery, H., Joyce, J., Smith, A.L., 1990. Late Jurassic to Late Cretaceous development of island arc crust in southwestern Puerto Rico. Transactions of the 12th Caribbean Geological Conference. The University of Miami, Miami FL, pp. 268–281.

Schiano, P., Clocchiatti, R., Shimizu, N., Maury, R.C., Jochum, K.P., Hoffman, A.W., 1995. Hydrous silica-rich melts in the sub-arc mantle and their relationship with erupted arc lavas. Nature 377, 594–600.

Sen, C., Dunn, T., 1994. Experimental modal metasomatism of a spinel lherzolite and the production of amphibole-bearing peridotite. Contributions to Mineralogy and Petrology 119, 422–432.

Shinjo, R., 1999. Geochemistry of high Mg andesites and the tectonic evolution of the Okinawa Trough–Ryukyu arc system. Chemical Geology 157, 69–88.

Slodowski, T.R., 1956. Geology of the Yauco area, Puerto Rico. Ph.D Dissertation, Princeton University, Princeton NJ.

Smith, A.L., Schellekens, J.H., Díaz, M., 1998. Batholith emplacement in the northeastern Caribbean: markers of tectonic change. Geological Society of America Special Paper 322, 99–122.

Stern, C.R., Kilian, R., 1996. Role of subducted slab, mantle wedge and continental crust in the generation of adakites from the Andean Austral Volcanic Zone. Contributions to Mineralogy and Petrology 123, 263–381.

Stimac, J., Hickmott, D., 1994. Trace-element partition-coefficients for ilmenite, orthopyroxene and pyrrhotite in rhyolite, detrermined by micro-pixe analysis. Chemical Geology 117, 313–330.

Sun, S.-S., McDonough, W.F., 1989. Chemical and isotopic systematics of oceanic basalts. Geological Society Special Publication 42, 313–345.

Tatsumi, Y., 1981. Melting experiments on a high-magnesian andesite. Earth and Planetary Science Letters 54, 357–365.

Tatsumi, Y., 2001. Geochemical modeling of partial melting of subducting sediments and subsequent melt–mantle interaction: generation of high-Mg andesites in the Setouchi volcanic belt, southwest Japan. Geology 29, 323–326.

Tatsumi, Y., Nakashima, T., Tamura, Y., 2002. The petrology and geochemistry of calc-alkaline andesites on Shido-Shima Island, SW Japan. Journal of Petrology 43, 3–16.

Tatsumi, Y., Shukuno, H., Sato, K., Shibata, T., Yoshikawa, M., 2003. The petrology and geochemistry of high-magnesium andesites at the western tip of the Setouchi Volcanic Belt, SW Japan. Journal of Petrology 44, 1562–1578.

Taylor, B., Martinez, F., 2003. Back-arc basin systematics. Earth and Planetary Science Letters 30, 481–497.

van Gestel, J.P., Mann, P., Grindlay, N.R., Dolan, J., 1999. Three-phase tectonic evolution of the northern margin of Puerto Rico as inferred from an integration of seismic, well, and outcrop data. Marine Geology 161, 259–288.

Viruete, J.E., Diaz de Neira, A., Huerta, P.P.H., Monthel, J., Senz, J.G., Joubert, M., Lopera, E.E., Ullrich, T., Friedman, R., Mortensen, J., Pérez-Estaún, A., 2006. Magmatic relationships and ages of Caribbean island arc tholeiites, boninites and related felsic rocks, Dominican Republic. Lithos 90, 161–186.

Volckmann, R.P., 1983. Upper Cretaceous stratigraphy of southwest Puerto Rico. United States Geological Survey Bulletin 1537-A.

Yogodzinski, G.M., Volynets, A.V., Koloskov, A.V., Seliverston, N.I., Matvenkov, V.V., 1994. Magnesian andesites and the subduction component in a strongly calc-alkaline series at Piip Volcano, Far Western Aleutians. Journal of Petrology 35, 163–204.

Yogodzinski, C.A., Kay, R.W., Volynets, O., Koloskov, A., Kay, S.M., 1995. Magnesian andesite in the western Aleutian Komandorsky region: implications for slab melting processes in the mantle wedge. Geological Society of America Bulletin 107, 505–519.